Primary Control Level of Parallel DER Converters in System of Multiple Interconnected Autonomous Microgrids within Self–Healing Networks

Farhad Shahnia[1], Ruwan P.S. Chandrasena[1], Sumedha Rajakaruna[1] and Arindam Ghosh[2]

[1]Center of Smart Grid and Sustainable Power Systems, Electrical and Computer Engineering Department, Curtin University, Perth, Australia

[2]School of Electrical Engineering and Computer Science, Queensland University of Technology, Brisbane, Australia.

(Corresponding Author: farhad.shahnia@curtin.edu.au Tel: +61–432020732)

***Abstract*—**In order to minimize the number of load shedding in a Microgrid (MG) during autonomous operation, islanded neighbor MGs can be interconnected if they are on a self–healing network and an extra generation capacity is available in the Distributed Energy Resources (DER) of one the MGs. In this way, the total load in the system of interconnected MGs can be shared by all the DERs within those MGs. However, for this purpose, carefully designed self–healing and supply restoration control algorithm, protection systems and communication infrastructure are required at the network and MG levels. In this paper, first a hierarchical control structure is discussed for interconnecting the neighbor autonomous MGs where the introduced primary control level is the main focus of this paper. Through the developed primary control level, this paper demonstrates how the parallel DERs in the system of multiple interconnected autonomous MGs can properly share the load of the system. This controller is designed such that the converter–interfaced DERs operate in a voltage–controlled mode following a decentralized power sharing algorithm based on droop control. DER converters are controlled based on a per–phase technique instead of a conventional direct–quadratic transformation technique. In addition, a linear quadratic regulator based state feedback controllers, which are more stable than conventional proportional integrator controllers, are utilized to prevent instability and weak dynamic performances of DERs when autonomous MGs are interconnected. The efficacy of the primary control level of DERs in the system of multiple interconnected autonomous MGs is validated through PSCAD/EMTDC simulations considering detailed dynamic models of DERs and converters.

Keywords: Interconnected Microgrids, Self–Healing Network, Power Sharing, DER, DSTATCOM.

1. INTRODUCTION

Smart Grid (SG) is a term referred to the improved condition of existing electric networks into more reliable, efficient, sustainable and customer interactive status by properly adding advanced metering, protection and communication infrastructures [1–2]. A general summary of the available SG definitions, standards, protection and management plans and the required information technology, energy and communication infrastructures are given in [1]. Among various anticipated smart features, self–healing is a key attribute in SGs. It is mainly driven by the requirement to improve system reliability [2–4]. In a self–healing network, it is expected that the network can continuously detect, analyze and respond to faults and restore feeders with minimum human intervention. Therefore, in case of a fault in the network, the normal operation can be restored in different feeder sections by properly isolating only the faulted subsections such that the amount of the affected loads is minimized. The feasibility study carried out in [5] concludes that integration of self–healing capabilities to the future SGs will bring high financial benefits for both utilities and customers by reducing the number of affected customers as well as the amount of unsupplied energy.

For a self–healing network, the intelligent agents are required to adapt the system operation conditions. These agents are then utilized for analyzing and maintaining the system reliability in real–time. A framework, required to implement autonomous agents throughout an interconnected system, was proposed in [6]. Such a framework can be utilized to support a self–healing SG through the system monitoring and controlling. Some self–healing reconfiguration techniques were proposed in [7–8] to divide the network into isolated grids while minimizing the number of effected loads. Some utilities in US have already started implementing self–healing projects [9].

Another key aspect of SG technology is increasing the participation of Distributed Energy Resources (DER) in electricity generation [3]. Microgrid (MG) is a cluster of DERs and loads which can operate in grid–connected mode as well as in autonomous (islanded) mode during planned (network maintenance) or unplanned (network fault) conditions [10]. A survey on MG control strategies is presented in [11].

In grid–connected mode, the grid dictates voltage and frequency of the network and DERs operate at their nominal (rated) capacities. The desired reference for DERs output can be derived using a constant PQ control strategy in this mode of operation [12]. Alternatively, in autonomous mode, if the DERs generation capacity is higher than local load demand, they will be sharing the loads. In this regard, voltage and frequency droop control strategy was

proposed in [13] for deriving the reference for the DER converters, for power sharing among parallel converter–interfaced DERs similar to the droop control technique used for power sharing among generators in a conventional power system. Later, voltage and angle droop was proposed in [14] to be used instead of the voltage and frequency droop for converter–interfaced DER applications. For improving the system response, the modified droop control was proposed in [15]. For improving the small signal stability, an arctan power frequency droop was proposed in [16] instead of the conventional droop method. Recently, intelligent power sharing algorithms such as adaptive droop control [17] and intelligent droop control [18] are proposed to remove the dependency of droop control on line parameters. In addition, in [19], a potential function based method was utilized instead of the droop control to adjust common set points required for power sharing among the DERs in a MG. Stability of the MG system with different power sharing algorithms is also investigated in [20–22]. Once the references for the DERs are assigned, the DER converters can be controlled either in voltage–controlled [23–24] or current–controlled [25–26] strategies to track the desired references.

In grid–connected mode, the grid dictates the network voltage; however, in autonomous mode, the network voltage can be indirectly regulated by the DERs based on the droop control. Although in both modes, the voltage along the Low Voltage (LV) network is maintained within acceptable limits, it is desired to hold the voltage to the nominal value of 1 pu. This can be achieved if one of the DERs in MG regulates the network voltage to 1 pu, referred to as Master DER in [11]. However, the DERs in residential LV networks are owned by customers and are not be responsible for network voltage support. This is because utilizing the converter of a DER to generate reactive power, for supporting the network voltage profile, will reduce the active power generation capacity of the converter which is not desired by their owners. Alternatively, a Distribution Static Compensator (DSTATCOM) can be used in each MG to regulate its Point of Common Coupling (PCC) voltage [27].

Another important issue in MGs is islanding detection and resynchronization. Islanding is referred to the isolating of MG from the grid. Different islanding detection methods are presented in [28]. In [28], it is indicated that a communication based method can be utilized to send the circuit breaker status from the circuit breaker to the DER converters. This method is the preferred method among other islanding detection methods since it has no None Detection Zones (NDZ). Resynchronization is referred to the reconnection process of a DER to MG or a MG to grid [29]. If a DER operates in current–controlled strategy, no resynchronization is required when connecting to

MG. However, if a DER operates in voltage–controlled strategy, proper resynchronization is required. Reconnection should only take place once the voltage magnitude difference and voltage phase difference across the respective circuit breaker is zero or lower than a very small specified value [29]. Inappropriate reconnection may cause high current fluctuations which can damage the network assets or result in system instability. Different resynchronisation methods were proposed in [30–32].

If DERs generation capacity in an autonomous MG is less than the local load demand, load shedding has to be carried out in order to maintain the voltage and frequency in the MG [33–34].

It is expected that in near future, there will be several MGs in each distribution network. They will be located in a neighborhood and the networks will be facilitated with self–healing capabilities. In such a scenario, an islanded operation of a MG is not anymore desired due to load shedding possibility. However, in such systems, the concept of microgrids supporting each other becomes more viable. The topic of "Interconnected MGs" or "Clusters of MGs" is the next stage of future research in distribution networks. In [35–36] based on the MG and power market concepts and availability of control and communication infrastructures, a model of distributed autonomous MGs was proposed. In such a model, if the DERs generation capacity in an autonomous MG is less than the local load demand but there is surplus generation capacity in DERs of neighbor autonomous MGs, interconnecting these two MGs can reduce the load shedding in the MG with deficiency of generation. In this model, the DERs in interconnected MGs should be properly controlled to share the total load demand in the interconnected system. With the increased interest in SG and self–healing networks, there will be a possibility of interconnecting autonomous MGs in the near future. The following assumptions are required when interconnecting two autonomous MGs:

- Availability of communication infrastructure among DERs, protection devices and circuit breakers,
- Self–healing capability in the network,
- Surplus generation capacity in the DER of one of the MGs,
- Possibility of bypassing some of the current technical requirements for DER interconnection.

The main contribution of this paper is developing the proper primary control level for DER converters in MGs such that interconnecting autonomous neighbor MGs will not result in undesired dynamic performance neither instability in DER outputs. In addition, a desired droop based load power sharing among all the DERs in the system of interconnected autonomous MGs is achieved. This is accomplished by applying a Linear Quadratic Regu-

lator (LQR) based technique for controlling the DER converters instead of the traditional Proportional–Integrator–Derivative (PID) based controllers. The main characteristic of PID based controllers is their dependency to network and load parameters. Therefore, tuning the PID control parameters is highly important to achieve an acceptable dynamic performance [37–39]. In the condition of interconnecting autonomous MGs, the initially tuned PID control parameters may not result in an acceptable dynamic performance and even may lead to instability. Therefore, an adaptive or intelligent PID controls are required which increase the complexity of the controller. However, LQR is an optimal and robust controller [39]; its control parameters only depend on the DER converter parameters and are independent from network and load characteristics. In addition, a per–phase (i.e. ABC) based control technique is utilized in this research instead of the traditional Direct–Quadrature (DQ) transformation in which a PID controller is not effective in tracking sinusoidal waveforms. Using the proposed per–phase control technique, even unbalanced systems can be phase controlled individually. These are the main advantages of the developed and proposed primary control level in this paper. Using the proposed and developed control technique, desired dynamic performance of DER converters is achieved in the scenarios of interconnecting autonomous MGs.

The rest of the paper investigates and validates the dynamic performance of DER converters in systems of interconnected autonomous MGs, when they are controlled based on the proposed and developed primary control algorithm. This forms the first stage of the interconnected MGs project. Developing and validating the control philosophy for interconnecting MGs as well as formulating the configuration and coordination of the required hardware, based on the transient performance of the system [40], are the next stages of this project. These issues are beyond the scope of this paper and will be addressed in a future publication.

2. NETWORK UNDER CONSIDERATION

Let us consider a Medium Voltage (MV) feeder connected to two LV MGs, namely MG–1 and MG–2, through distribution transformers T_1 and T_2, as shown in Fig. 1(a). MG–1 has 3 DERs (i.e. DER_1 to DER_3) and 5 loads while MG–2 has 2 DERs (i.e. DER_4 to DER_5) and 4 loads. A DSTATCOM is installed at the secondary side of the distribution transformer in each MG to regulate the voltage at its PCC. The loads are assumed to be residential loads and all DERs are assumed to be converter–interfaced DERs.

During grid connected mode, all DERs will be operating at their rated capacities or the capacities desired by the economic analyses. During planned maintenance or unplanned fault situations on the MV feeder, the MGs will work in autonomous mode. In this mode, when CB_{M1} and CB_{M2} are open, the DERs of each MG will be sharing the loads of that MG separately. Now, if the load demand in each MG is higher than the power generation capacity of the DERs in that MG, load shedding must be applied to some of the (non–critical) loads in that MG.

Now, let us assume a scenario in which the power generation in MG–2 is less than its demand; while the power generation capacity in DERs of MG–1 is higher than its demand. Assuming the network has self–healing and automatic supply restoration capability, CB_{M1} and CB_{M2} can be closed while CB_G will remain open. In this way, the two MGs will be interconnected together. Hence, the DERs in MG–1 can share some of the loads in MG–2 and prevent/reduce load shedding in MG–2.

This paper focuses only on validating the dynamic performance of DER converters in the system of interconnected neighbor autonomous MGs, with the proposed control scheme. It is to be noted that developing and validating the control philosophy for interconnecting neighbor MGs and the required hardware are beyond the scope of this paper and will be addressed in future publications. Sections below present a brief explanation on modeling the network.

2.1 DER and Converter Structure and Modeling

The considered DERs in this paper are photovoltaic cells (PV), fuel cells and batteries, connected to the MG through Voltage Source Converters (VSC). Detailed dynamic models of these micro sources are utilized in this research. These models were presented by the authors in [15,41] and are not repeated here.

The considered DERs have a VSC consisting of three single–phase H–bridges, as shown in Fig. 1(b). This VSC structure has better controllability and dynamic performance under unbalanced conditions in the network compared to VSCs with three–phase three–leg or four–leg configurations; since in this configuration, each phase is controlled individually.

Each H–bridge of VSCs is composed of IGBTs with proper parallel reverse diode and snubber circuits. The outputs of each H–bridge are connected to a single–phase transformer, with $1 : a$ ratio, and the three transformers are star–connected. The transformers provide galvanic isolation as well as voltage boosting. In this figure, the re-

sistance R_f represents the switching and transformer losses, while the inductance L_f represents the leakage reactance of the transformers. The filter capacitor C_f is connected to the output of the transformers to bypass the switching harmonics.

2.2 Network Voltage Regulation

As mentioned in Section 1, in grid connected mode, the grid dictates the network voltage and in autonomous mode, the DERs indirectly regulate the network voltage based on the droop control. Although in both modes, the voltage along the LV network will be within acceptable limits, it is desired to hold the network voltage to its nominal value of 1 pu. For this, in this paper, voltage regulation in the MGs is achieved by a DSTATCOM installed at the secondary side of the distribution transformer in each MG, which regulates its PCC voltage to a desired value, by exchanging reactive power with the network. The implemented DSTATCOM has the same converter structure as those of the DERs and its control is discussed in Section 3.4.

2.3 MG Resynchronization

As mentioned in Section 1, in this research, resynchronization of a DER to MG and a MG to grid is required as DERs are operating in voltage–controlled strategy. For resynchronisation, the voltage magnitude and angle are measured on both sides of the circuit breaker. A Phase–Locked Loop (PLL) is utilised for measuring the voltage angle [29]. The circuit breaker closes once the voltage angles and magnitudes are the same on both sides. However, based on network load and parameters, resynchronization can be slow and may take from several milliseconds to minutes [31].

It is to be noted that resynchronisation can be a complicated process depending on the network configuration, existence of systems of interconnected MGs and their location along the MV feeder [40]. Therefore, a general resynchronisation, self–healing and automatic supply restoration algorithm is required for this purpose. This controller will utilise communications between the network circuit breakers. This is beyond the scope of the research in this paper and will be addressed in a future publication.

3. NETWORK AND MICROGRID CONTROL

For proper operation of a MG within a network, where the interconnection of neighbor MGs are considered, a three–level hierarchical control system [19,42–43], shown in Fig. 1(e), is required as discussed below:

- The primary (lowest) control level consists of inner–loop and outer–loop controls. Inner–loop control is responsible for appropriate switchings in the converter such that a proper tracking of the desired reference in DER converter output is achieved. This control is based on the references determined by outer–loop control and the local current and voltage measurements in DER converter output. Outer–loop control is responsible for proper output power control of DERs in the MG. This control generates the proper references for the inner–loop control and is different for grid–connected and autonomous modes. The dynamic performance of DER converters in the system of interconnected MGs depends on the primary control level which is the main focus of this paper and is discussed further in Sections 3.1–3.3.
- The secondary control is the central controller of the MG. This controller sends the desired (reference) output power of each DER converter to them. In grid–connected mode, the desired output power of each DER converter is received from the tertiary controller. However, in autonomous mode, this controller sends reference signals to DER converters in the form of voltage magnitude and angle, based on monitoring the network voltage and frequency, whenever required. This controller runs in a slower time frame compared to that of the primary control [19]. It is to be noted that in the proposed system, the DSTATCOMs are operating individually based on their pre–default set points and are not controlled by the secondary controller. The secondary control is beyond the scope of this research and is not discussed in this paper.
- The tertiary (highest) control communicates with the central controllers in each MG and the protection devices and circuit breakers of the network. In general, this controller can utilize load forecasting, electricity market and demand response information for optimal power flow of the network and MGs [44]. Additionally, in case of a network with self–healing capability, this controller utilizes the information received from the circuit breakers to define the network configuration and status. In this case, MGs coordination agent decides whether interconnection of neighbor MGs is required and if any, identifies those MGs. Then, using the self–healing and supply restoration agent, it decides which circuit breakers should open/close and sends the proper commands to them. This controller also monitors the network data and decides whether two interconnected MGs

should be isolated and sends the proper commands to the relevant circuit breakers to operate. As mentioned before, designing the tertiary control with its sub agents requires an extensive study and will be addressed in a future publication.

3.1 Outer–Loop Control in Grid–connected Mode

Let us consider the DERs have a VSC and filter structure as shown in Fig. 1(b) with its equivalent single–phase circuit as shown in Fig. 1(c). This equivalent circuit can also be represented by its Thevenin equivalent parameters (i.e. V_{Th} and Z_{Th}) as shown in Fig. 1(d). From Fig. 1(d), it can be seen that the instantaneous active power (p) and reactive power (q) supplied from DER–i to its PCC can be expressed as [45]

$$
\begin{aligned}
p_i &= \frac{\left(|V_{T,i}||V_{Th,i}|\cos\phi_i - |V_{Th,i}|^2\right)\cos\theta_i + |V_{T,i}||V_{Th,i}|\sin\phi_i\sin\theta_i}{|Z_{Th,i} + Z_{coup,i}|} \\
q_i &= \frac{\left(|V_{T,i}||V_{Th,i}|\cos\phi_i - |V_{Th,i}|^2\right)\sin\theta_i - |V_{T,i}||V_{Th,i}|\sin\phi_i\cos\theta_i}{|Z_{Th,i} + Z_{coup,i}|} \\
\phi_i &= \delta_{Th,i} - \delta_{T,i} \\
\theta_i &= \angle\left(Z_{Th,i} + Z_{coup,i}\right)
\end{aligned}
\tag{1}
$$

where V_T is the PCC voltage, Z_{coup} is the coupling impedance and $V = |V|\angle\delta$ represents the phasor notation of $v(t)$. It is to be noted that the coupling impedance is dominantly inductive (i.e. $Z_{coup} \approx j\omega L_{coup}$). In Section 3.3, it will be shown that after applying the proposed converter control, Z_{Th} is dominantly inductive in 50 Hz (i.e. $Z_{Th} \approx j\omega L_{conv}$) and has a very small magnitude. Therefore, it is expected that $V_{Th} \approx V_{cf}$ in Fig 1(d) where V_{cf} is the voltage across the capacitor C_f. Based on these assumptions, (1) can be simplified as

$$
\begin{aligned}
p_i &= \frac{|V_{T,i}||V_{cf,i}|\sin\left(\delta_{cf,i} - \delta_{T,i}\right)}{\omega L_{conv,i} + \omega L_{coup,i}} \\
q_i &= \frac{|V_{T,i}||V_{cf,i}|\cos\left(\delta_{cf,i} - \delta_{T,i}\right) - |V_{T,i}|^2}{\omega L_{conv,i} + \omega L_{coup,i}}
\end{aligned}
\tag{2}
$$

The average active power (P) and reactive power (Q) supplied by each DER can then be calculated from p and q using a low pass filter.

In grid–connected mode, the grid dictates voltage and frequency of the network and the DERs operate at their nominal (rated) capacities. This can be achieved using a constant PQ control mode of operation [12]. In this paper, a voltage–controlled technique is utilized which will monitor the PCC voltage (V_T) to regulate DER converter output voltage (V_{cf}) such that the desired nominal active and reactive power are injected into the network. For this, the PCC voltage magnitude and angles should be measured instantaneously and used in (2) to calculate the converter output reference voltage ($V_{cf,ref}$) for the desired powers and the known coupling inductance. This reference voltage will later be used in the inner–loop control to generate the switching signals for the converter. The schematic diagram of this control is shown in Fig. 1(f).

3.2 Outer–Loop Control in Autonomous Mode

During autonomous mode, network voltage and frequency should be regulated by the DERs. In addition, a proper power sharing among the DERs is desired. Below, a detailed description of the designed and implemented power sharing algorithm based on droop control is given.

Let us now consider a MG with 2 parallel converter–interfaced DERs supplying a common load. DER–1 is connected to the load through a feeder impedance of $Z_{line,1}$ where DER–2 is connected to the load through a feeder impedance of $Z_{line,2}$. Let us also assume the feeder is highly inductive (i.e. $Z_{line} \approx j\omega L_{line}$). Assuming the voltage at load PCC is V_{load}, the active and reactive power supplied from each DER to the load can be expressed as

$$p_i = \frac{|V_{load,i}||V_{cf,i}|\sin(\delta_{cf,i} - \delta_{load,i})}{\omega L_{conv,i} + \omega L_{coup,i} + \omega L_{line,i}}$$
$$q_i = \frac{|V_{load,i}||V_{cf,i}|\cos(\delta_{cf,i} - \delta_{load,i}) - |V_{load,i}|^2}{\omega L_{conv,i} + \omega L_{coup,i} + \omega L_{line,i}} \quad (3)$$

As the feeder is assumed to be highly inductive, the active and reactive powers are decoupled and a DC load flow analysis can be applied. In addition, the angle difference between V_{cf} and V_{load} is small. Based on DC load flow, the average active power supplied from each DER to the load is

$$P_i = \frac{|V_{load,i}||V_{cf,i}|(\delta_{cf,i} - \delta_{load})}{\omega L_{conv,i} + \omega L_{coup,i} + \omega L_{line,i}} \quad (4)$$

To supply the load with an average active power of P_i , from (4), the angle of the voltage across the filter capacitor of DER–*i* will be

$$\delta_{cf,i} = P_i\left(\Gamma_{conv,i} + \Gamma_{coup,i} + \Gamma_{line,i}\right) + \delta_{load} \tag{5}$$

where $\Gamma_i = \dfrac{\omega L_i}{\left|V_{cf,i}\right|\left|V_{load}\right|}$

Decentralized power sharing among several DERs in a MG can be achieved by changing the voltage magnitude and angle of DERs using the droop control as [18]

$$\begin{aligned}\delta_{cf,i} &= \delta_{rated,i} - m_i\left[\frac{X_{line}}{Z_{line}}\left(P_{rated,i} - P_i\right) - \frac{R_{line}}{Z_{line}}\left(Q_{rated,i} - Q_i\right)\right] \\ \left|V_{cf,i}\right| &= V_{rated,i} - n_i\left[\frac{R_{line}}{Z_{line}}\left(P_{rated,i} - P_i\right) + \frac{X_{line}}{Z_{line}}\left(Q_{rated,i} - Q_i\right)\right]\end{aligned} \tag{6}$$

where V_{rated} and δ_{rated} are respectively the rated voltage magnitude and angle of the DER when supplying rated active power (P_{rated}) and reactive power (Q_{rated}). Reactive power–voltage and active power–angle droop coefficients are represented by *n* and *m*, respectively. As the feeder lines are assumed to be inductive, (6) can be further simplified as

$$\begin{aligned}\delta_{cf,i} &= \delta_{rated,i} - m_i\left(P_{rated,i} - P_i\right) \\ \left|V_{cf,i}\right| &= V_{rated,i} - n_i\left(Q_{rated,i} - Q_i\right)\end{aligned} \tag{7}$$

This is monitored and controlled in the MG through the outer–loop control. Therefore, it is expected that the outer–loop control determines the desired V_{cf} for each DER in MG. The block diagram of outer–loop control is shown in Fig. 1(f).

Let us assume when each DER changes its output active power from zero to its nominal (rated) capacity, the DER frequency reduces by $\Delta\omega$. Based on this assumption, the active power–angle droop coefficient for each DER [46] is derived from

$$m_i = \frac{\Delta\omega}{P_{rated,i}} \tag{8}$$

Assuming $\Delta\omega$ to be constant for DERs *i* and *j* with different nominal capacities, we have

$$\frac{m_i}{m_j} = \frac{P_{rated,j}}{P_{rated,i}} \tag{9}$$

Now, let us assume that all DERs in the MG have the same power factor and when each DER changes its output reactive power from zero to its nominal (rated) capacity, the DER voltage reduces by ΔV. Based on this assumption, the reactive power–voltage droop coefficient for each DER [46] is derived from

$$n_i = \frac{\Delta V}{Q_{rated,i}} \tag{10}$$

Assuming ΔV to be constant for DERs *i* and *j* with different nominal capacities, we have

$$\frac{n_i}{n_j} = \frac{Q_{rated,j}}{Q_{rated,i}} \tag{11}$$

Now, for the MG in steady state condition, let us assume DER–*i* and DER–*j* have the same δ_{rated}. Therefore, from (7) and (9) we have

$$\delta_{cf,i} - \delta_{cf,j} = \left(\delta_{rated,i} - \delta_{rated,j}\right) - m_i\left(P_{rated,i} - P_i\right) + m_j\left(P_{rated,j} - P_j\right) = m_i P_i - m_j P_j \tag{12}$$

Replacing $\delta_{cf,i}$ and $\delta_{cf,j}$ from (5) in (12), we have

$$P_i\left(\Gamma_{conv,i} + \Gamma_{coup,i} + \Gamma_{line,i}\right) - P_j\left(\Gamma_{conv,j} + \Gamma_{coup,j} + \Gamma_{line,j}\right) = m_i P_i - m_j P_j \tag{13}$$

Therefore, the ratio of the active power supplied by the DERs is equal to

$$\frac{P_j}{P_i} = \frac{-m_i + \Gamma_{conv,i} + \Gamma_{coup,i} + \Gamma_{line,i}}{-m_j + \Gamma_{conv,j} + \Gamma_{coup,j} + \Gamma_{line,j}} \tag{14}$$

Eq. (14) shows that output active power of each DER is inversely proportional to the sum of Γ in its output. The three components of Γ_{conv}, Γ_{coup} and Γ_{line} are dependent on three inductances between the DER and the load. Since Γ has a parameter of voltage square in its denominator, it is expected that

$$\Gamma_{conv,i} \ll \Gamma_{line,i} \ll \Gamma_{coup,i} \ll m_i \tag{15}$$

Therefore, (14) can be simplified further as

$$\frac{P_j}{P_i} \approx \frac{m_i}{m_j} \tag{16}$$

In a similar way, it can be shown that the ratio of the reactive power supplied by the DERs in the MG will be

$$\frac{Q_j}{Q_i} \approx \frac{n_i}{n_j} \tag{17}$$

Hence, based on the above assumption, from (9), (16) and (11), (17), it is expected that the output active and reactive power ratio among two DERs in the MG will be same as the ratio of their nominal active and reactive power capacities.

On the other hand, in parallel operation of converter–interfaced DERs in a MG, it is desired that, for all the DERs, the voltage angle difference across their coupling inductances (i.e. $\delta_{cf} - \delta_T$) in (2) to be constant. This voltage angle difference is preferred to be small [46] so that it is on the linear section of sinusoidal P–δ characteristic of (2). Similarly, it is desired that the voltage drop across the coupling inductances (i.e. $|V_{cf}| - |V_T|$) in (2) to be constant, for all the DERs. This voltage drop is preferred to be small and in the range of 1–2 % [47]. For achieving these assumptions, the coupling inductances are designed inversely proportional to the nominal power ratio of DERs as

$$\frac{L_{coup,i}}{L_{coup,j}} = \frac{P_{rated,j}}{P_{rated,i}} = \frac{Q_{rated,j}}{Q_{rated,i}} \tag{18}$$

From (1)–(18), it is concluded that for an accurate power sharing among DERs in MG, we require

$$\begin{aligned} \frac{P_j}{P_i} &\approx \frac{m_i}{m_j} = \frac{L_{coup,i}}{L_{coup,j}} = \frac{P_{rated,j}}{P_{rated,i}} \\ \frac{Q_j}{Q_i} &\approx \frac{n_i}{n_j} = \frac{L_{coup,i}}{L_{coup,j}} = \frac{Q_{rated,j}}{Q_{rated,i}} \end{aligned} \tag{19}$$

3.3 Inner–Loop Control

As mentioned before, the outer–loop control regulates the output power of DERs by adjusting the proper references for the each DER from (2) or (7). The inner–loop control will calculate and apply proper switching signals for the IGBTs in the DER converter such that the desired voltage ($V_{cf,ref}$) is perfectly generated across the AC filter capacitor (C_f).

It is desired to develop a per–phase based control technique (i.e. ABC) instead of the conventional DQ transformation based techniques. For this, let us consider the equivalent single–phase circuit of VSC as shown in Fig.

1(c). In this figure, $u{\cdot}a{\cdot}V_{dc}$ represents the converter output voltage, where u is the switching function. For a 2–level (bipolar) switching, u can take on ±1 value which will be used subsequently to turn ON/OFF the IGBTs.

Let us consider the DER converter and its output filter as system for which a controller is to be developed. The differential equations that describe the dynamic behavior of this system are given by

$$\begin{aligned} u_i.a.Vdc &= R_f i_{f,i} + L_f \frac{di_{f,i}}{dt} + v_{cf,i} \\ i_{f,i} &= C_f \frac{dv_{cf,i}}{dt} + i_{T,i} \end{aligned} \tag{20}$$

A closed–loop optimal linear robust controller based on state feedback is utilized to generate u. Let us assume the state vector $x(t)$ for each phase of the system is defined as

$$x_i(t) = [v_{cf,i}(t) \quad i_{f,i}(t)]^T \tag{21}$$

where $v_{cf}(t)$ represent the instantaneous voltage across AC filter capacitor, $i_f(t)$ is the current passing through filter inductor L_f and T is the transpose operator. Then, the equivalent circuit of this system can be represented with state space equation of

$$\dot{x}_i(t) = A x_i(t) + B_1 u_{c,i}(t) + B_2 i_{T,i}(t) \tag{22}$$

where

$$A = \begin{bmatrix} 0 & \frac{1}{C_f} \\ -\frac{1}{L_f} & -\frac{R_f}{L_f} \end{bmatrix} \quad B_1 = \begin{bmatrix} 0 \\ \frac{a.Vdc}{L_f} \end{bmatrix} \quad B_2 = \begin{bmatrix} -\frac{1}{C_f} \\ 0 \end{bmatrix} \tag{23}$$

In (22), $u_c(t)$ is the continuous time version of switching function u and i_T represents the network load change effects on this system; hence it is assumed as a disturbance for the controller.

In the control systems, the desired values for each control parameter in steady state condition must be known. However, it is rather hard to determine the reference for i_f in (21). Nevertheless, it is desired that i_f has only low frequencies. Therefore, instead of using i_f as a control parameter, its high frequency components ($\tilde{i}_f$) can be used in the control system. Based on this assumption, $\tilde{i}_f$ can be described and expanded in Laplace domain as [48]

$$\tilde{i}_f(s) = \frac{s}{s+\alpha} i_f(s) = \left(1 - \frac{\alpha}{s+\alpha}\right) i_f(s) = i_f(s) - \hat{i}_f(s) \tag{24}$$

where α is the cut–off frequency of this high–pass filter and $\hat{i}_f$ is the low frequency components of i_f which is given by

$$\hat{i}_f(s) = \frac{\alpha}{s+\alpha} i_f(s) \tag{25}$$

Eq. (25) can be expressed in differential equation form as

$$\frac{d\hat{i}_f(t)}{dt} = \alpha\left(i_f(t) - \hat{i}_f(t)\right) \tag{26}$$

Now, let us define a new state vector for the system, which includes $\hat{i}_f$, as [48]

$$x_i'(t) = [v_{cf,i}(t) \quad i_{f,i}(t) \quad \hat{i}_{f,i}(t)]^T \tag{27}$$

In this case, the system can be represented with new state space equation of

$$\dot{x}_i'(t) = A' x_i(t) + B_1' u_{c,i}(t) + B_2' i_{T,i}(t) \tag{28}$$

where

$$A' = \begin{bmatrix} 0 & \frac{1}{C_f} & 0 \\ -\frac{1}{L_f} & -\frac{R_f}{L_f} & 0 \\ 0 & \alpha & -\alpha \end{bmatrix} \quad B_1' = \begin{bmatrix} B_1 \\ 0 \end{bmatrix} \quad B_2' = \begin{bmatrix} B_2 \\ 0 \end{bmatrix} \tag{29}$$

Eq. (28) can be represented in discrete–time domain as [39]

$$x_i'(k+1) = Fx_i'(k) + G_1 u_{c,i}(k) + G_2 i_{T,i}(k) \tag{30}$$

where

$$F = e^{A'.T_s} \quad , \quad G_1 = \int_0^{T_s} e^{A't} B_1' \, dt \quad , \quad G_2 = \int_0^{T_s} e^{A't} B_2' \, dt \tag{31}$$

where T_s is the sampling time. From (30), $u_c(k)$ can be computed, using a suitable state feedback control law, as

$$u_{c,i}(k) = -K[x_i'(k) - x_{ref,i}'(k)] \tag{32}$$

where K is a gain matrix and $x'_{ref}(k)$ is the desired state vector for (27), in discrete–time mode.

It is to be noted that the desired reference value for $v_{cf}(t)$ for each DER will be determined by the outer–loop control. This value is calculated from (2) when MG operates in grid–connected mode and from (7) when MG op-

erates in autonomous mode. As mentioned before, the desired reference value for $\tilde{i}_f(t)$ for all DERs is always set to zero to minimize the high frequency components of the current flowing through L_f. Therefore, $i_f(t)$ must only contain low frequency components (i.e. $i_f(t) = \hat{i}_f(t)$). Now, the reference vector, X'_{ref} can be defined for each DER as

$$X'_{ref,i} = [V_{cf,ref,i} \quad \hat{I}_f \quad \hat{I}_f]^T = [V_{cf,i} \angle \delta_{cf,i} \quad \hat{I}_f \quad \hat{I}_f]^T \tag{33}$$

As the system behavior in steady–state is interested and assuming a full control over $u_c(k)$, an infinite time LQR [39] can be designed for this problem to define K. This controller is more stable than PID based controls and prevents the instability among parallel DERs when two autonomous MGs interconnect together. In addition, PID based controllers are not very effective when utilized in per–phase based controls.

In a discrete LQR problem, an objective function J is chosen as

$$J_i(k) = \sum_{k=0}^{\infty} \left[\left(x'_i(k) - x'_{ref,i}(k) \right)^T Q_i(k) \left(x'_i(k) - x'_{ref,i}(k) \right) + u_i(k)^T R_i(k) u_i(k) \right] \tag{34}$$

where R is the control cost matrix, Q is the state weighting matrix which reflects the importance of each controlling parameter in x and $J(\infty)$ represents the objective function at infinite time (steady–state condition) for the system. Eq. (34) is then minimized to obtain the optimal control law $u(k)$ through solution of steady state Riccati equations [39] while satisfying system constraints in (30). The LQR method ensures the desired results for the system while the variations of system load and source parameters are within acceptable limits of reality.

Eq. (32) shows the total tracking error of each DER converter. The tracking error can be minimized by limiting this error within a very small bandwidth (e.g. $h = \pm 10^{-4}$). Now, from (32), for each DER, the switching function u (i.e. which pairs of IGBTs to turn ON/OFF) is generated using a hysteresis control based on the error level as

$$\begin{aligned} &\textit{If} \quad u_{c,i}(k) > +h \quad \textit{then} \quad u_i = +1 \\ &\textit{If} \quad -h \le u_{c,i}(k) \le +h \quad \textit{then} \quad u_i = \textit{previous } u_i \\ &\textit{If} \quad u_{c,i}(k) < -h \quad \textit{then} \quad u_i = -1 \end{aligned} \tag{35}$$

More detail on the discussed converter control is given in [27].

To achieve a good tracking of the output voltage, a state feedback control was utilized for each DER. Therefore, the controller expression can be presented as

$$u_i.a.Vdc = v_{cf,ref,i} - K(X'_i - X'_{ref,i}) = v_{cf,ref,i} - k_1\left(v_{cf,i} - v_{cf,ref,i}\right) - k_2\left(\tilde{i}_{f,i} - 0\right) \tag{36}$$

where $K = [k_1 \;\; k_2 \;\; k_2]$ is the gain matrix in (32).

Replacing (36) in (20) and representing that in Laplace domain, we have

$$V_{cf,i}(s)\left[L_f C_f s^2 + R_f C_f s + 1\right] + I_{T,i}(s)\left[L_f s + R_f\right] = V_{cf,ref,i}(s)\left[k_1 + 1\right] - k_1 V_{cf,i}(s) - \frac{k_2 s}{s+\alpha} I_{f,i}(s) \tag{37}$$

From (37), the parameters of the Thevenin equivalent circuit of the DER converter and filter including the developed state feedback control are given by

$$V_{cf,i}(s) = G_1(s) V_{cf,ref,i}(s) + G_2(s) I_{T,i}(s) \tag{38}$$

where $G_1(s)$ and $G_2(s)$ are defined as

$$G_1(s) = \frac{(k_1+1)s + \alpha(k_1+1)}{L_f C_f s^3 + C_f\left(R_f + k_2 + \alpha L_f\right)s^2 + \left(k_1 + 1 + \alpha R_f C_f\right)s + \alpha(k_1+1)}$$

$$G_2(s) = \frac{L_f S^2 + \left(R_f + \alpha L_f - k_2\right)S + \alpha R_f}{L_f C_f s^3 + C_f\left(R_f + k_2 + \alpha L_f\right)s^2 + \left(k_1 + 1 + \alpha R_f C_f\right)s + \alpha(k_1+1)} \tag{39}$$

and $G_1(s)\, V_{cf,ref}(s) = V_{Th}$ and $G_2(s) = -Z_{Th}$.

The performance of the state feedback control versus the open loop transfer function of the DER converter and filter system can be studied from frequency domain behavior. For this, the Bode diagram of $G_1(s)$ and $G_2(s)$ are obtained and shown in Figs. 2(a) and (b), respectively. In Fig. 2(a), it can be seen that at frequency range of interest (i.e. 50 Hz), $G_1(s)$ has the property of a unity gain with zero angle (i.e. $V_{Th} \approx V_{cf}$). This helped us to simplify (1) into (2) in Section 3.1. On the other hand, in Fig. 2(b), it can be seen that at frequency range of interest, $G_2(s)$ magnitude is relatively high in open loop condition. The high value takes the network load and i_T change effects into the DER converter control. This magnitude is reduced effectively by properly designing the state feedback gains. It is to be noted that $G_2(s)$ is relatively inductive around 50 Hz. This is the reason for assuming Z_{Th} to be pure inductive in (1) in Section 3.1.

3.4 DSTATCOM Control

As discussed in Section 2.2, voltage regulation in this MG is achieved by a DSTATCOM installed at the secondary side of the distribution transformer, which regulates its PCC voltage to a desired value. The utilized

DSTATCOM in this paper has an LCL filter in its converter output and voltage regulation is achieved by exchanging reactive power with the network. The reactive power exchange can be controlled in two different methods. These two methods are discussed below and a detailed discussion is provided in Appendix A about the benefits and limitations of each control method when several DSTATCOMs are installed on a MV feeder.

- Voltage control strategy: The first method is based on directly controlling the PCC voltage. In this method, the difference between the PCC RMS voltage ($V_{T-DSTAT}$) and its desired value ($V_{T-DSTAT,desired}$) is utilized to generate the required voltage magnitude across AC filter capacitor in DSTATCOM as

$$\left|V_{cf-DSTAT}\right| = V_{cf-DSTAT,ref} + \left(K_P + \frac{K_I}{s}\right)\left(V_{T-DSTAT,desired} - V_{T-DSTAT}\right) \tag{40}$$

  where $V_{cf-DSTAT,ref}$ is the assumed reference value for this voltage, K_P and K_I are PI controller parameters and the suffix *DSTAT* represents DSTATCOM.

- Power factor correction strategy: The second method is based on power factor correction at PCC. This method is not a direct voltage control method since the DSTATCOM is controlled to exchange a desired reactive power with the network ($Q_{DSTAT,ref}$) which is equal to the network reactive power demand in downstream side of the DSTATCOM. Hence, the required voltage magnitude across AC filter capacitor in DSTATCOM can be calculated as

$$\left|V_{cf-DSTAT}\right| = V_{cf-DSTAT,ref} + \left(K'_P + \frac{K'_I}{s}\right)\left(Q_{DSTAT,ref} - Q_{DSTAT}\right) \tag{41}$$

  where Q_{DSTAT} is the measured injected reactive power by the DSTATCOM.

The DC capacitor voltage (V_{dc}) in DERs is stabilized by their DC sources; however, there is no such a DC source in DSTATCOMs. V_{dc} in DSTATCOM can be kept equal to its reference value ($V_{dc,ref}$) when the AC system does not exchange any power with the DC capacitor [49]. This can be reassured if the AC system replenishes the DSTATCOM converter losses. For this, the angle of the voltage across the AC filter capacitor (δ_{cf}) must be varied with respect to the DC capacitor voltage variations as

$$\delta_{cf-DSTAT,ref} = \left(K''_P + \frac{K''_I}{s}\right)\left(V_{dc-DSTAT,ref} - V_{dc-DSTAT}\right) \tag{42}$$

4. STUDY CASES AND SIMULATION RESULTS

For investigating the dynamic performance of DER converters in the system of interconnected MGs within a self–healing network, different simulation cases are considered. This performance is investigated in various operating conditions, in PSCAD/EMTDC. Some of the simulation results are discussed below while the network parameters are given in Appendix B.

It is to be noted that the following case studies are considering LV MGs with the loads and DERs in the range of a few kWs. However, the proposed concept is valid for MV MGs with the DERs and loads in the range of several MWs and similar studies can also be performed for such scenarios.

4.1. Case 1: Microgrid Operation in Grid–Connected and Autonomous Modes

Let us consider the system of Fig. 1(a) to investigate the DERs operation during grid–connected and autonomous modes of MGs. In grid–connected mode, each DER will generate its rated power and the extra load demand will be supplied by the grid or the DER extra generation will flow back into the grid. In autonomous mode, the load demand of each MG is shared among the DERs of that MG proportional to their rating.

The operation of only MG–1 is investigated in this section. For this, let us assume in the system of Fig. 1(a), CB_G and CB_{M1} are closed while CB_{M2}, CB_{S1} and CB_{S2} are open. The system is assumed to be in steady state condition at t = 0 s and all the DERs are running at their rated conditions. The DSTATCOM is not connected to the system.

At t = 1 s, the grid is disconnected (i.e. CB_G is opened) and MG–1 starts to operate in autonomous mode. Therefore, the DERs increase their output power to satisfy the load demand within the MG. At t = 2 s a 25% load increase (i.e. 3 kW) and at t = 3 s a load decrease of 25% are applied in the MG. It can be seen that all DERs are sharing the load change proportional to their ratings. At t = 4 s, it is desired that MG reconnect to the grid. In order to prevent fluctuations in the current and power, the resynchronization method described in Section 2.3 is used. The resynchronization is achieved at t = 10.1 s and CB_G closes. It can be seen the system reaches to the steady state condition after each change within 5 cycles. Fig. 3(a) shows the active power dispatch of grid and 3 existing DERs in MG–1 between 0 and 11 seconds in the above–mentioned network while Fig. 3(b) shows the reactive power dispatch within the same time period.

The voltage profile of the network is also shown in Fig. 3(c). As it can be seen in this figure, during the autonomous mode, there might be an uncontrolled voltage drop/rise in the network, as none of the DERs are regulating the network voltage. In this paper, a DSTATCOM is utilized to regulate the network voltage. To investigate the efficacy of DSTATCOM, let us now assume that in Fig. 1(a), CB_{S1} is closed and DSTATCOM–1 is connected. For this condition, the active and reactive power dispatch of grid and DERs are shown in Figs. 4(a) and (b), respectively. The voltage profile of the network is now highly improved to the desired value of 1 pu, as shown in Fig. 4(c). The difference in the active powers in figures 3(a) and 4(a) is due to the fact that voltage was varying before DSTATCOM installation. The voltage profile of DSTATCOM DC capacitor is shown in Fig. 4(d) which has a negligible drop of 1% in autonomous mode. The output active and reactive power of DSTATCOM is also shown in Fig. 4(e). The oscillations in the results of Fig. 4 are due to the dynamic characteristics of DSTATCOM. It is also to be noted that the resynchronization mechanism is similar to the previous case and not shown here.

4.2. Case 2: System of Interconnected Autonomous Microgrids

Let us assume that in system of Fig. 1(a), at t = 0 s, circuit breakers CB_G, CB_{M1}, CB_{M2}, CB_{S1} and CB_{S2} are closed and the network is at steady state condition. The considered system has self–healing capability. Now, let us also assume, due to a fault in the MV grid, after self–healing process, CB_G is open while CB_{M1} and CB_{M2} are closed at t = 1. As mentioned before, the operation of the protection devices and circuit breakers and resynchronization of interconnecting MGs during self–healing process is beyond the scope of this paper. In this paper, this transition period is not considered. At t = 2 s a load increase of 25% and at t = 3 s a load decrease of 25% are also applied in MG–1.

The total active power supply from the grid in addition to the active power flow into each MG is shown in Fig. 5(a). From this figure, it can be seen that MG–2 has a negative power flow and is delivering, approximately, 20% of the load demand in MG–1. The active power output of all the DERs in MG–1 and MG–2 are shown separately in Figs. 5(b) and (c), respectively. It can be seen that all DERs in MG–1 and MG–2 are sharing the load demand of the system of interconnected MGs proportional to their ratings. The voltage profile in the secondary side of the distribution transformers in each MG is regulated to the desired value of 1 pu as shown in figures 5(d) and (e).

The active and reactive power drawn by a sample load in the network, with a 2.7 kW demand and power factor of 0.95, is also shown in Fig. 5(f).

Now, let us assume another case in which the two DERs in MG–2 are running in their maximum capacity (i.e. 4 and 8 kW, respectively). Let us also assume at t = 1, due to a fault in the MV grid and after self–healing process, CB_G is open while CB_{M1} and CB_{M2} are closed. It is to be noted that the self–healing transition period is not considered in this study. A 25% load increase and decrease in the network is applied at t = 2 and 3 s, respectively.

For this case, the total active power supply from the grid in addition to the active power flow into each MG is shown in Fig. 6(a). From this figure, it can be seen that MG–1 has a negative power flow and is delivering, approximately, 30% of the load demand in MG–2. The active power output of all the DERs in MG–1 and MG–2 are shown separately in Figs. 6(b) and (c), respectively. It can be seen that all DERs in MG–2 are running in their maximum rating at all times while the DERs in MG–1 are sharing the rest of the network load demand proportional to their ratings.

4.3. Case 3: Large MV Feeder with Several Systems of Interconnected Microgrids

Now, let us assume a larger MV feeder with self–healing capability with the single line diagram as shown in Fig. 7. The assumed network contains 9 MGs which can be interconnected at certain times to fulfill the power demand requirement of each other. Each MG is a combination of several DERs and loads plus a DSTATCOM at the secondary side of their distribution transformer.

The network is divided into 3 zones by proper installation and coordination of circuit breakers CB_G, CB_{M1}, CB_{M2} and CB_{M3}, as shown in this figure. This zone forming can be achieved by deploying the required protection and communication infrastructure, which is not the scope of this paper.

Now, let us assume at t = 0 s the network is in steady state condition and all the circuit breakers are closed. In case of a fault within any MG, the faulty MG can be isolated from the rest of the network by the proper operation of the LV circuit breaker, located in the secondary side of the distribution transformer, of the relevant MG. let us assume at t = 0.5 s, a fault is occurred on the MV feeder which is cleared at t = 1 s. Based on the fault location, three separate cases are assumed as below:

Case 3.1: The fault is on the MV feeder within Zone–2.

Case 3.2: The fault is on the MV feeder within Zone–1.

Case 3.3: The fault is on the MV grid (i.e. upstream of Zone–1).

For case 3.1, when the fault is within Zone–2, it is expected that, based on the protection and circuit breaker co-ordination and self–healing process, CB_{M2} to be opened while all other circuit breakers are closed. In such a case, the DERs in MG–5, MG–6 and MG–7 have to independently supply their local load demand and a load shedding is required if their generation capacity is less than their load demand. At t = 1 s, CB_{M2} is reclosed after the fault is cleared. Fig. 8 shows the simulation results for the network in this case. The active power supplied from the grid in addition to the power supplied to Zone–2 and Zone–3 are shown individually in Fig. 8(a). The active power flow into each MG feeder is also shown for all three zones separately, in figures 8(b) to (d). From Fig. 8(c), it can be seen that the active power flow into the MGs within Zone–2 becomes zero between 0.5 and 1 second as CB_{M2} is opened, while no power variation is observed in Zone–1 and Zone–3 MGs.

For case 3.2, when the fault is within Zone–1, it is expected CB_G and CB_{M1} to be opened while all other circuit breakers are closed. In such a case, the DERs in MG–1 to MG–4 have to independently supply their local load demand. However, as Zone–2 and Zone–3 MGs are interconnected, they can share the load demand altogether and this will prevent or reduce the load shedding for the loads of these two zones. Fig. 9 shows the simulation results for the network in this case. The active power supplied from the grid in addition to the power supplied to Zone–2 and Zone–3 are shown individually in Fig. 9(a). The active power flow into each MG feeder is also shown for all three zones separately, in figures 9(b) to (d). From the simulation results, it can be seen that the active power flow into the MGs within Zone–1 becomes zero between 0.5 and 1 second as CB_G and CB_{M1} are opened. In addition, it can be seen that the DERs in MG–6, MG–8 and MG–9 have negative power flow. This indicates that these MGs are delivering some portion of the loads within MG–5 and MG–7 in addition to their local loads. If this interconnection was not possible, then load shedding was inevitable for MG–5 and MG–7.

For case 3.3, when the fault is in the upstream of Zone–1, it is expected only CB_G to be opened while all other circuit breakers are closed. In such a case, the MGs in all three zones are interconnected and their DERs will share the load demand altogether. Hence, the load shedding for the loads of these three zones will be prevented or reduced. Fig. 10 shows the simulation results for the network in this case. The active power supplied from the grid

in addition to the power supplied to Zone–2 and Zone–3 are shown individually in Fig. 10(a). The active power flow into each MG feeder is also shown for all three zones separately, in figures 10(b) to (d). From the simulation results, it can be seen that the active power flow supplied by the grid becomes zero between 0.5 and 1 second as CB_G is opened. Therefore, all DERs in the MGs will increase their output power to pick up the required extra demand. From the simulation results, it can be seen that MG–3 and MG–9 have zero active power flow. This indicates that all the generation capacity of their DERs is consumed by their local loads. On the other hand, it can be seen that MG–2, MG–4 and MG–8 have negative power flow. This indicates that these MGs are delivering some portion of the loads within MG–1, MG–5, MG–6 and MG–7 in addition to their local loads. If this interconnection was not possible, then load shedding was inevitable for these MGs. This verifies the efficacy of the proposed operation and control of the DER converters in the system of interconnected MGs.

5. CONCLUSION

The primary control level for the DER converters in the system of interconnected neighbor autonomous MGs within a SG network with self–healing capability was proposed. In such a system, if the DER generation capacity in an autonomous MG is less than the local load demand but there is surplus generation capacity in the DERs of the neighbor autonomous MGs, interconnecting these MGs can reduce the load shedding. A hierarchical control system was described for the network and MG levels. The concepts of self–healing and supply restoration algorithm, protection devices and their coordination and communication belong to the tertiary control level and were not the focus of this paper. This paper focused on the primary control level which guarantees a proper power sharing among all the DERs in the system of interconnected MGs. Control algorithms were developed to manage the parallel operation of converter–interfaced DERs at grid–connected and autonomous operation modes in the MGs while the network voltage was regulated by the DSTATCOMs installed in each MG. Using the developed inner loop and outer loop control techniques, an acceptable dynamic performance of DER converters in transients and steady–state conditions was achieved. The proposed method prevented any undesired voltage, power and frequency variations in the network. Based on the described primary control level, a DER with extra generation capacity can successfully share some of the loads in other MGs, once the other MGs have a shortage of generation.

APPENDIX A–Parallel Operation of Multiple DSTATCOMs

In this section, a short discussion is given on voltage correction and power factor correction strategies for DSTATCOMs when several DSTATCOMs are installed in a MV feeder. Let us now assume a radial MV network supplying 5 distribution transformers with a LV feeder in their downstream. All feeders have a similar impedance load of 88 kW and power factor of 0.95. They are located at equal distances from each other. We refer to them as Feeder–1 to Feeder–5. The network does not include any DERs or DSTATCOMs. In this case, voltage profile of the MV feeder is dropped from 0.97 pu, at the beginning of the feeder, to 0.92 pu, at the end of the feeder, as shown in Table 1.

Now, let us assume there is a DSTATCOM connected to the secondary side of each distribution transformers. The operation of each DSTATCOM is independent from other DSTATCOMs and they all operate in voltage control strategy. Once a DSTATCOM regulates its PCC voltage, the voltage in the primary side of that transformer is also regulated accordingly. Hence, in the assumed MV feeder, the DSTATCOMs can be utilized such that they regulate the voltage, along the MV feeder, to a desired voltage profile. This voltage profile can be chosen as a flat voltage line (i.e. 1 pu for all DSTATCOMs), in the most ideal case. Another possibility, is choosing a gradually decreasing voltage drop line (e.g. 1, 0.99,…, 0.96 pu). These set points are allocated for each DSTATCOM during commissioning period and do not change continuously. It is also to be noted that no optimization method is utilized to select these set points in this analysis. Note that since the DSTATCOMs hold the voltage along the feeder, the node voltages are not affected by load changes.

The voltage profile in the primary and secondary side of the transformers for both of these cases is given in Table 1. From this table, it can be seen that they both have similar result in the voltage profile in the MV feeder. However, it can be seen that in the case of flat voltage profile, the amount of injected reactive power by DSTATCOMs installed at feeder end nodes are higher than that of the DSTATCOMs installed at feeder beginning nodes. Therefore, the DSTATCOMs at feeder end nodes have a relatively higher rating compared to DSTATCOMs in feeder beginning nodes in the case of a flat voltage profile compared to the gradually decreasing voltage drop line. On the other hand, at the beginning of the MV feeder, a huge reverse reactive power flow is observed in the case of the flat voltage line which is reduced in the other case, as given in Table 2.

Now, let us assume that all DSTATCOMs are operating in power factor correction strategy. In this case, they will all inject the required reactive power by the loads in their downstream. As the loads have similar impedances and the voltage drops from the beginning of the MV feeder towards the end, the amount of the injected reactive power by the DSTATCOMs slightly decreases from the beginning of the feeder towards the end. However, the voltage profile is improved compared to the case without DSTATCOMs, as shown in Table 1. On the other hand, no reverse reactive power flow is also observed at the beginning of the MV feeder, as shown in Table 2.

Based on this discussion, controlling DSTATCOMs with power factor correction strategy results in indirect improved voltage profile in both MV and LV feeders, prevents reverse reactive power flow in MV feeder and minimizes the rating of DSTATCOMs.

APPENDIX B– Network Data and Parameters

The parameters of the networks under consideration are given in Tables 3 and 4.

REFERENCES

[1] K. Moslehi and R. Kumar, "A reliability perspective of the smart grid," *IEEE Trans. on Smart Grid*, Vol. 1, No. 1, pp. 57–64, Jun. 2010.

[2] X. Fang, S. Misra, G. Xue and D. Yang, "Smart grid– The new and improved power grid: A survey," *IEEE Communications Surveys & Tutorials*, Vol. 14, No. 4, pp. 944–980, 2012.

[3] H. Liu, X. Chen, K. Yu and Y. Hou, "The control and analysis of self–healing urban power grid,", *IEEE Trans. on Smart Grid*, Vol. 3, No. 3, pp. 1119–1129, Sep. 2012.

[4] M. Kezunovic, "Smart fault location for smart grids," *IEEE Trans. on Smart Grid*, Vol. 2, No. 1, pp. 11–22, March 2011.

[5] K. Moslehi, A.B.R. Kumar and P. Hirsch, "Feasibility of a self–healing grid– Part II: Benefit models and analysis," IEEE Power Engineering Society General Meeting, pp. 1–8, 2006.

[6] A. Zidan, E.F. El–Saadany, "A Cooperative multiagent framework for self–healing mechanisms in distribution systems," *IEEE Trans on Smart Grid*, Vol. 3, No. 3, pp. 1525–1539, Sept. 2012.

[7] S.A. Arefifar, Y.A.I. Mohamed and T.H.M. EL–Fouly, "Supply–adequacy–based optimal construction of microgrids in smart distribution systems," *IEEE Trans. on Smart Grid*, Vol. 3, No. 3, pp. 1491–1502, Sept. 2012.

[8] A. Košťálová and P.M.S. Carvalho, "Towards self–healing in distribution networks operation: Bipartite graph modeling for automated switching," *Electric Power Systems Research*, Vol. 81, Issue 1, pp. 51–56, Jan. 2011.

[9] R.J. Yinger, "Self–healing circuits at southern California Edison," IEEE Transmission and Distribution Conference and Exposition, pp. 1–3, May 2012.

[10] N. Hatziargyriou, H. Asano, R. Iravani and C. Marnay, "Microgrids," *IEEE Power and Energy Magazine*, Vol. 5, No. 4, pp. 78–94, 2007.

[11] W. Huang, M. Lu and L. Zhang, "Survey on Microgrid Control Strategies," *Energy Procedia*, Vol. 12, pp. 206–212, 2011.

[12] J.A.P. Lopes, C.L. Moreira and A.G. Madureira, "Defining control strategies for Microgrids islanded operation," *IEEE Trans. on Power Systems*, Vol. 21, No. 2, pp. 916–924, 2006.

[13] M.C. Chandorkar, D.M. Divan and R. Adapa, "Control of parallel connected inverters in standalone AC supply systems," *IEEE Trans. Industrial Application*, Vol. 29, No. 1, pp. 136–143, 1993.

[14] R. Majumder, A. Ghosh, G. Ledwich and F. Zare, "Angle droop versus frequency droop in a voltage source converter based autonomous microgrid," IEEE Power Engineering Society General Meeting, pp.1–8, 2009.

[15] R. Majumder, F. Shahnia, A. Ghosh, G. Ledwich, M. Wishart and F. Zare, "Operation and control of a microgrid containing inertial and non–inertial micro sources," IEEE Region 10 Conference (TENCON), pp. 1–6, 2009.

[16] C.N. Rowe, T.J. Summers, R.E. Betz, D.J. Cornforth and T.G. Moore, "Arctan power–frequency droop for improved Microgrid stability," *IEEE Trans. on Power Electronics*, Vol. 28, No. 8, pp. 3747–3759, 2013.

[17] E. Rokrok and M.E.H. Golshan, "Adaptive voltage droop scheme for voltage source converters in an islanded multibus microgrid," *IET Generation Transmission and Distribution*, Vol. 4, No. 5, pp. 562–578, May 2010.

[18] H. Bevrani and S. Shokoohi, "An intelligent droop control for simultaneous voltage and frequency regulation in islanded microgrids," *IEEE Trans. on Smart Grid*, (in Press), doi:10.1109/TSG.2013.2258947.

[19] M.J. Sanjari and G.B. Gharehpetian, "Small signal stability based fuzzy potential function proposal for secondary frequency and voltage control of islanded microgrid," *Electric Power Components and Systems*, Vol. 41, No. 5, pp. 485–499, Feb. 2013.

[20] B. Johnson, A. Davoudi, P. Chapman, and P. Sauer, "A unified dynamic characterization framework for microgrid systems," *Electric Power Components and Systems*, Vol. 40, No. 1, pp. 93–111, Nov. 2011.

[21] C.X. Dou, D.L. Liu, X.B. Jia and F. Zhao, "Management and Control for Smart Microgrid Based on Hybrid Control Theory," *Electric Power Components and Systems*, Vol. 39, No. 8, pp. 813–832, Apr. 2011.

[22] R. Majumder, "Some aspects of stability in microgrids," *IEEE Trans. on Power Systems*, (in Press), doi: 10.1109/TPWRS.2012.2234146.

[23] R. Majumder, B. Chaudhuri, A. Ghosh, R. Majumder, G. Ledwich and F. Zare, "Improvement of stability and load sharing in an autonomous microgrid using supplementary droop control loop," *IEEE Trans. on Power Systems*, Vol. 25, No. 2, pp. 796–808, 2010.

[24] H. Nian and R. Zeng, "Improved control strategy for stand–alone distributed generation system under unbalanced and non–linear loads," *IET Renewable Power Generation*, Vol. 5, No. 5, pp. 323–331, Sep. 2011.

[25] F. Katiraei and M.R. Iravani, "Power management strategies for a microgrid with multiple distributed generation units," *IEEE Trans. on Power Systems*, Vol. 21, No. 4, pp. 1821–1831, 2006.

[26] A. Yazdani and R. Iravani, "A unified dynamic model and control for the voltage–sourced converter under unbalanced grid conditions," *IEEE Trans. on Power Delivery*, Vol. 21, No. 3, pp. 1620–1629, 2006.

[27] A. Ghosh and G. Ledwich, *Power quality enhancement using custom power devices*, Kluwer Academic Publishers, 2002.

[28] R. Teodorescu, M. Liserre and P. Rodriguez, *Grid converters for photovoltaic and wind power systems*, Wiley, 2011.

[29] F. Blaabjerg, R. Teodorescu, M. Liserre and A.V. Timbus, "Overview of control and grid synchronization for distributed power generation systems," *IEEE Trans. on Industrial Electronics*, Vol. 53, No. 5, pp. 1398–1409, Oct. 2006.

[30] J. Rocabert, G. Azevedo, I. Candela, R. Teoderescu, P. Rodriguez and I.E. Otadui, "Microgrid connection management based on an intelligent connection agent," IEEE 36th Annual Conf. on Industrial Electronics (IECON), pp. 3028–3033, Nov. 2010.

[31] R. Majumder, A. Ghosh, G. Ledwich and F. Zare, "Control of parallel converters for load sharing with seamless transfer between grid connected and islanded modes," IEEE Power Engineering Society General Meeting, pp. 1–7, 2008.

[32] T.L. Vandoorn, B. Meersman, J.D.M. De Kooning, L. Vandevelde, "Transition from islanded to grid–connected mode of microgrids with voltage–based droop control," *IEEE Trans. on Power Systems*, (in Press), doi: 10.1109/TPWRS.2012.2226481.

[33] Y.Y. Hong, M.C. Hsiao, Y.R. Chang, Y.D. Lee and H.C. Huang, "Multiscenario underfrequency load shedding in a microgrid consisting of intermittent renewables," *IEEE Trans. on Power Delivery*, (in Press), doi: 10.1109/TPWRD.2013.2254502.

[34] K. Seethalekshmi, S.N. Singh and S.C. Srivastava, "A synchrophasor assisted frequency and voltage stability based load shedding scheme for self–healing of power system," *IEEE Trans. on Smart Grid*, Vol. 2, No. 2, pp. 221–230, June 2011.

[35] R.H. Lasseter, "Smart distribution: Coupled microgrids," *Proceedings of the IEEE*, Vol. 99, No. 6, pp. 1074–1082, 2011.

[36] S. Rahman, M. Pipattanasomporn and Y. Teklu, "Intelligent distributed autonomous power systems (IDAPS)," IEEE Power Engineering Society General Meeting, pp. 1–8, 2007.

[37] H. Bevrani, *Robust Power System Frequency Control*, Springer, 2009.

[38] B. Pal and B. Chaudhuri, *Robust Control in Power Systems*, Springer, 2005.

[39] A. Tewari, *Modern Control Design with Matlab and Simulink*, Wiley, 2002.

[40] V. Spitsa, X. Ran, R. Salcedo, J.F. Martinez, R.E. Uosef, F. de Leon, D. Czarkowski and Z. Zabar, "On the transient behavior of large–scale distribution networks during automatic feeder reconfiguration," *IEEE Trans. on Smart Grid*, Vol. 3, No. 2, pp. 887–896, June 2012.

[41] F. Shahnia, R. Majumder, A. Ghosh, G. Ledwich and F. Zare, "Operation and control of a hybrid microgrid containing unbalanced and nonlinear loads," *Electric Power System Research*, Vol. 80, No. 8, pp. 954–965, Aug. 2010.

[42] J.J. Justo, F. Mwasilu, J. Lee and J.W. Jung, "AC–microgrids versus DC–microgrids with distributed energy resources: A review," *Renewable Sustainable Energy Reviews*, Vol. 24, pp. 387–405, Aug. 2013.

[43] J.M. Guerrero, J.C. Vasquez, J. Matas, L.G. de Vicuna and M. Castilla, "Hierarchical control of droop–controlled ac and dc microgrids—A general approach toward standardization," *IEEE Trans. on Industrial Electronics*, Vol. 58, No. 1, pp. 158–172, 2011.

[44] F. Katiraei, R. Iravani, N. Hatziargyriou and A. Dimeas, "Microgrids management," *IEEE Power Energy Magazine*, Vol. 6, No. 3, pp. 54–65, 2008.

[45] J.C. Vasquez, R.A. Mastromauro, J.M. Guerrero and M. Liserre, "Voltage support provided by a droop–controlled multifunctional inverter," *IEEE Trans. on Industrial Electronics*, Vol. 56, No. 11, pp. 4510–4519, Nov. 2009.

[46] R.H. Lasseter and P. Piagi, *Control and design of microgrid components*, Final project report, Power Systems Engineering Research Center, University of Wisconsin–Madison, 2006.

[47] A.M. Salamah, S.J. Finney and B.W. Williams, "Autonomous controller for improved dynamic performance of AC grid, parallel–connected, single–phase inverters," *IET Generation Transmission and Distribution*, Vol. 2, No. 2, pp. 209–218, Mar. 2008.

[48] A. Ghosh and G. Ledwich, "High bandwidth voltage and current control design for voltage source converters," 20th Australasian University Power Engineering Conference (AUPEC), pp. 1–6, 2010.

[49] A. Ghosh and G. Ledwich, "Load compensating DSTATCOM in weak AC systems," *IEEE Trans. on Power Delivery*, Vol. 18, No. 4, pp. 1302–1309, Oct. 2003.

List of Embedded Tables and Figures

(b) Active power output of each DER in MG–1,

(c) Active power output of each DER in MG–2,

(d) MG–1 voltage profile monitored in the secondary side of distribution transformer,

(e) MG–2 voltage profile monitored in the secondary side of distribution transformer,

(f) Active and reactive power demand of a sample load.

Fig. 6. Simulation results for the system of interconnected MG–1 and MG–2 when MG–2 DERs operate in their maximum capacity:

(a) Active power supply from grid and active power flow into each microgrid feeder,

(b) Active power output of each DER in MG–1,

(c) Active power output of each DER in MG–2,

Fig. 7. Schematic diagram of the large MV feeder with self–healing capability containing several interconnected microgrids.

Fig. 8. Simulation results for the network in case 3.1:

(a) Active power supply from grid and active power flow into Zone–2 and Zone–3,

(b) Active power flow into each microgrid within Zone–1,

(c) Active power flow into each microgrid within Zone–2,

(d) Active power flow into each microgrid within Zone–3.

Fig. 9. Simulation results for the network in case 3.2:

(a) Active power supply from grid and active power flow into Zone–2 and Zone–3,

(b) Active power flow into each microgrid within Zone–1,

(c) Active power flow into each microgrid within Zone–2,

(d) Active power flow into each microgrid within Zone–3.

Fig. 10. Simulation results for the network in case 3.3:

(a) Active power supply from grid and active power flow into Zone–2 and Zone–3,

(b) Active power flow into each microgrid within Zone–1,

(c) Active power flow into each microgrid within Zone–2,

(d) Active power flow into each microgrid within Zone–3.

Table 1. Numerical results of the analysis for different DSTATCOM control strategies.

	Operation Mode	Feeder 1	Feeder 2	Feeder 3	Feeder 4	Feeder 5
	No DSTATCOM	0.97	0.96	0.94	0.93	0.92
Secondary Voltage [pu]	Flat Voltage	1	1	1	1	1
	Gradually Decreased	1	0.99	0.98	0.97	0.96
	Power Factor Correction	0.98	0.96	0.95	0.94	0.94
Primary Voltage [pu]	Flat Voltage	0.98	0.97	0.97	0.96	0.96
	Gradually Decreased	0.98	0.97	0.96	0.96	0.95
	Power Factor Correction	0.98	0.96	0.95	0.94	0.94
Q_{DSTAT} [kVAr]	Flat Voltage	51.37	66.36	76.51	82.62	85.65
	Gradually Decreased	55.98	59.02	56.97	50.43	39.11
	Power Factor Correction	28.69	27.79	27.16	26.76	26.38

Table 2. Reactive power flow from Grid to the MV feeder, measured at the beginning of the feeder, for different DSTATCOM control strategies [kVAr].

No DSTATCOM	Flat Voltage	Gradually Decreased Voltage	Power Factor Correction
170.75	–160.07	–73.73	41.33

Table 3. Technical data of the network under consideration in Fig. 1.

MV Network	11 kV L–L RMS, 50 Hz
MV Line Impedances	R = 0.2 Ω, L =10 mH
LV Feeder	410 V L–L RMS, 50 Hz
LV Line Impedances	R = 0.02 Ω, L =1 mH
Transformers	30 kVA, 11 kV/ 410 V, Three–Phase, Δ / Y–Grounded, Z_I = 5%,
Impedance Loads	7 three–phase RL load each P = 3 kW, PF = 0.95
Induction Motors	2 three–phase each P =1.5 kW, PF = 0.8
DER VSCs and Filters	R_f = 0.1 Ω, L_f = 0.4 mH, C_f = 50 μF, V_{dc} = 150 V, a = 3.33, $h = 10^{-4}$
DSTATCOM VSCs and Filters	R_f = 0.1 Ω, L_f = 4 mH, C_f = 25 μF, V_{dc} = 1 kV, a = 1, $h = 10^{-4}$

Table 4. Technical data of the DERs and droop control coefficients for the network under consideration in Fig. 1.

DER Type	DER Rating [kW]	Coupling Inductance (L_{coup}) [mH]	m [rad/kW]	n [V/kVAr]
Fuel Cell (DER–1, 4)	4	5.61	1.5708	4.5
PV (DER–2, 5)	3	7.48	2.0944	6.0
Battery (DER–3)	2	11.22	3.1416	9.0

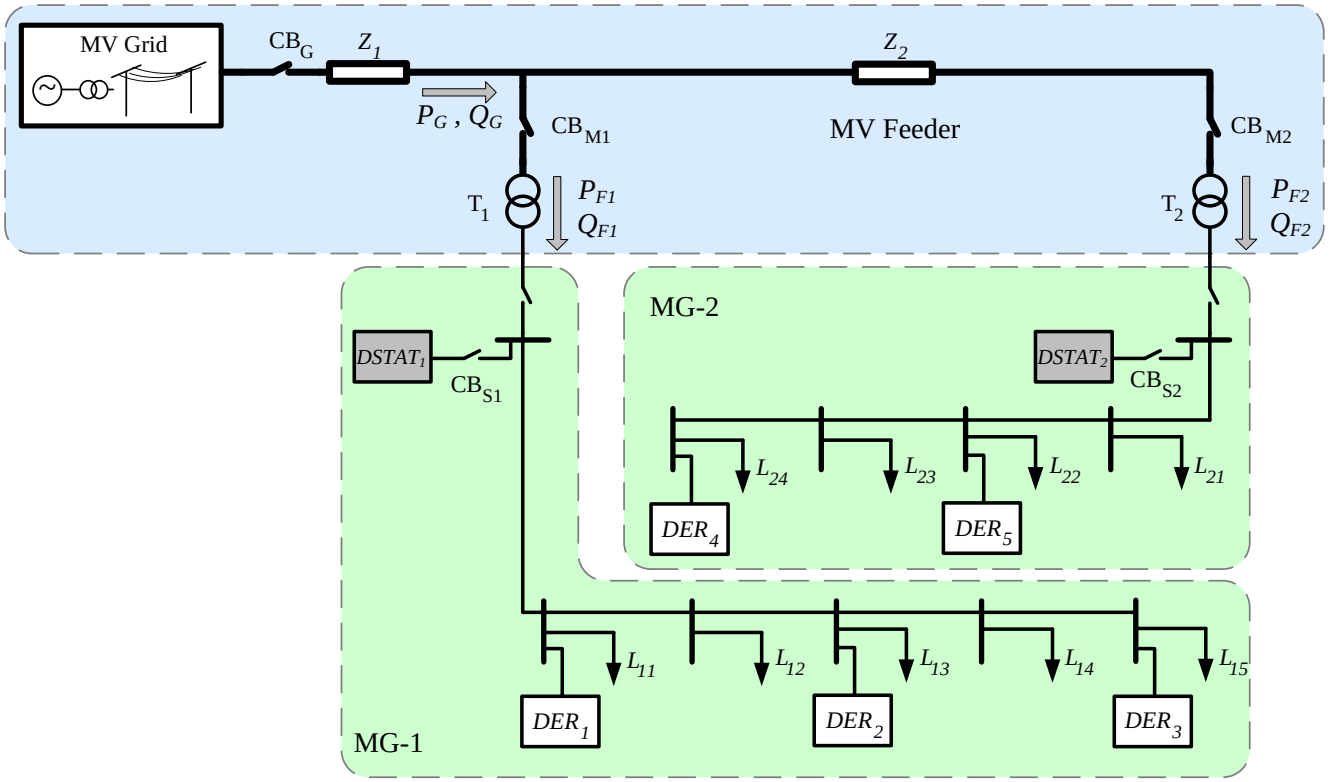
MV Grid
CB_G
Z_1
Z_2
P_G , Q_G
CB_M1
MV Feeder
CB_M2
T_1
P_F1
Q_F1
T_2
P_F2
Q_F2
MG-2
DSTAT_1
CB_S1
DSTAT_2
CB_S2
L_24
L_23
L_22
L_21
DER_4
DER_5
L_11
L_12
L_13
L_14
L_15
DER_1
DER_2
DER_3
MG-1

(a)

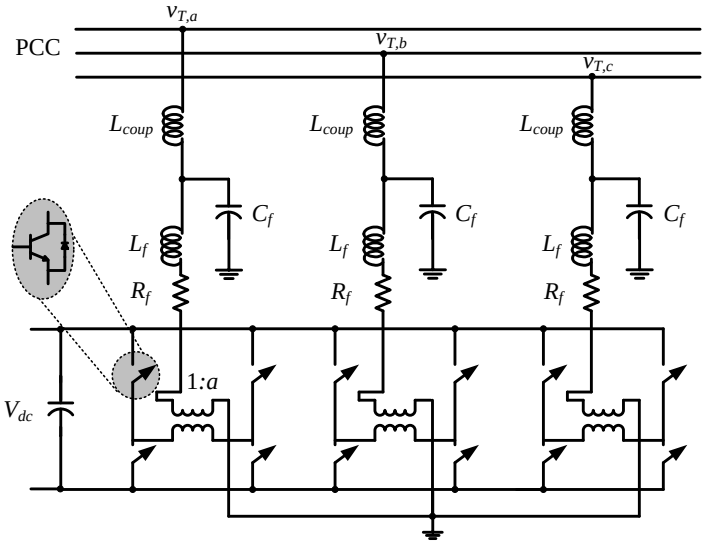
PCC
v_T,a
v_T,b
v_T,c
L_coup
C_f
L_f
R_f
1:a
V_dc

(b)

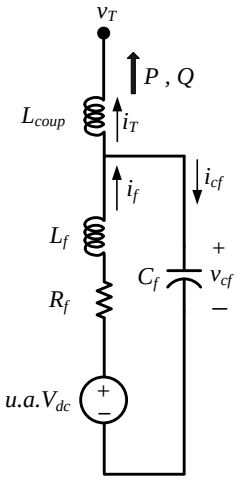
v_T
P , Q
L_coup
i_T
i_f
i_cf
L_f
R_f
C_f
+
v_cf
–
u.a.V_dc

(c)

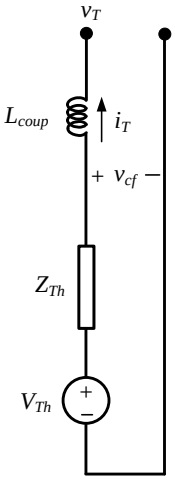
v_T
L_coup
i_T
+ v_cf –
Z_Th
V_Th

(d)

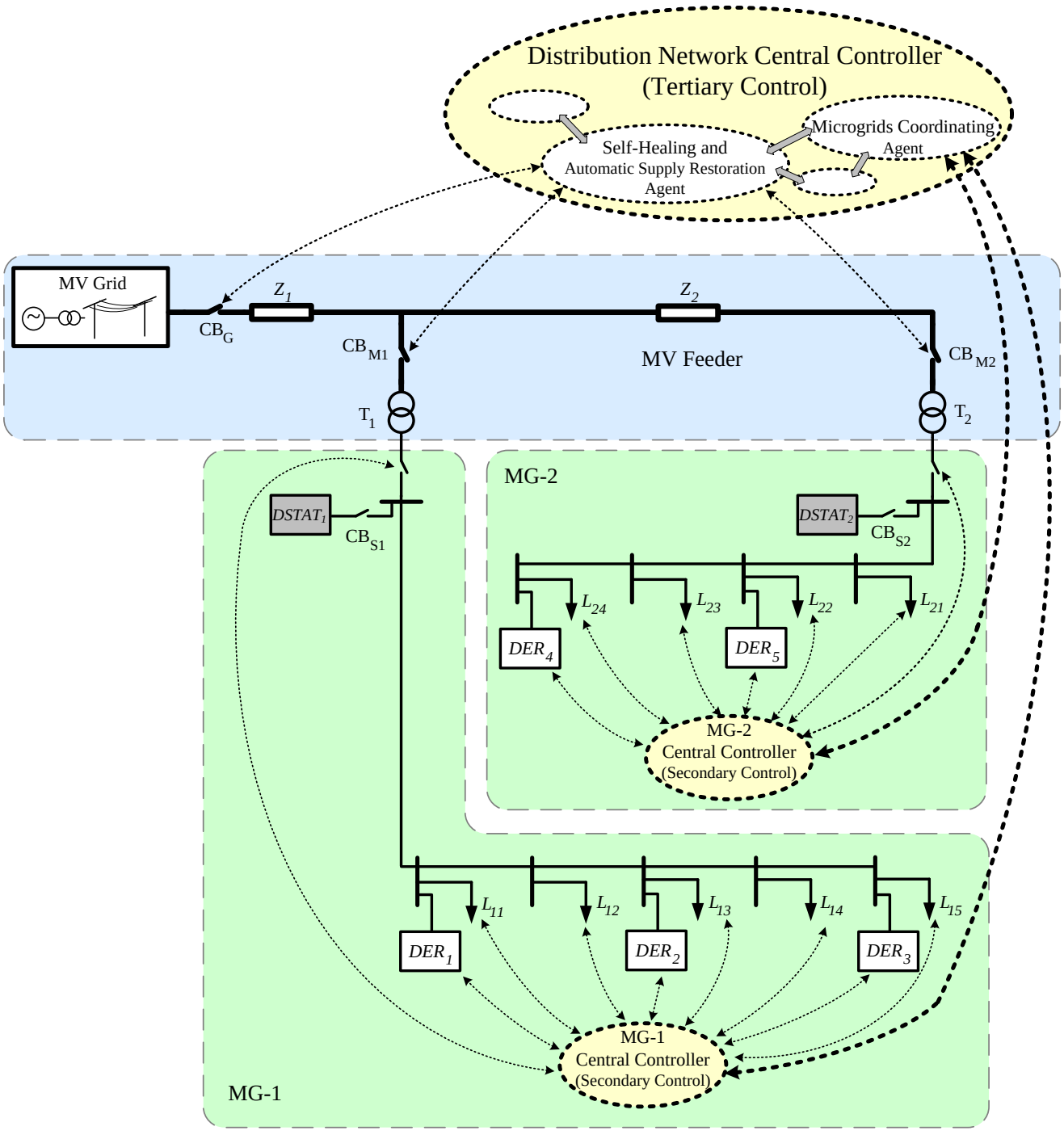
Distribution Network Central Controller
(Tertiary Control)
Self-Healing and
Automatic Supply Restoration
Agent
Microgrids Coordinating
Agent
MV Grid
Z1
Z2
CBG
CBM1
CBM2
MV Feeder
T1
T2
MG-2
DSTAT1
CBS1
DSTAT2
CBS2
L24
L23
L22
L21
DER4
DER5
MG-2
Central Controller
(Secondary Control)
L11
L12
L13
L14
L15
DER1
DER2
DER3
MG-1
Central Controller
(Secondary Control)
MG-1

(e)

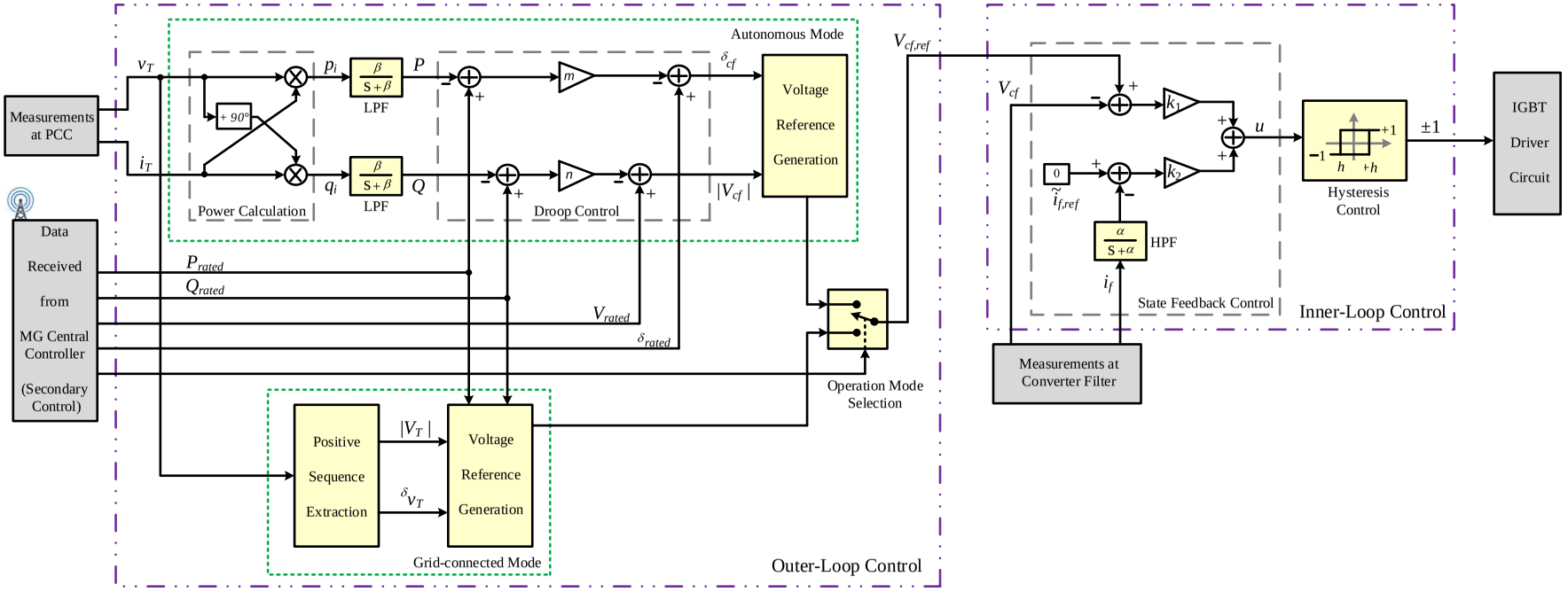

(f)

Fig. 1. (a) Schematic diagram of the network and microgrid structure under consideration,

(b) VSC and filters structure for DERs and DSTATCOMs,

(c) Single–phase equivalent circuit of VSC and filters,

(d) Thevenin equivalent circuit of VSC and filters,

(e) Hierarchical control structure,

(f) The block diagram of primary control level (outer and inner–loop controls).

(a)

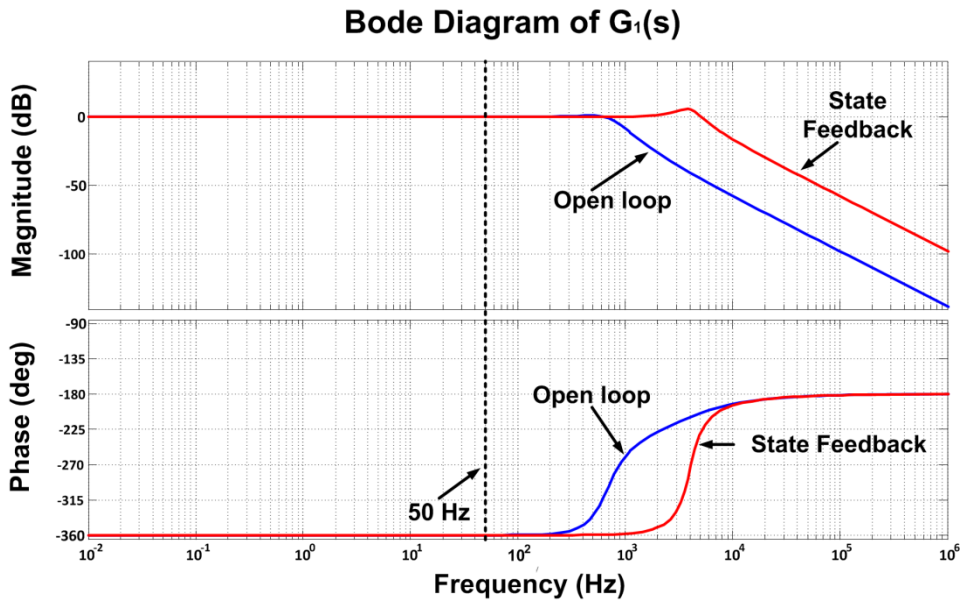

(b)

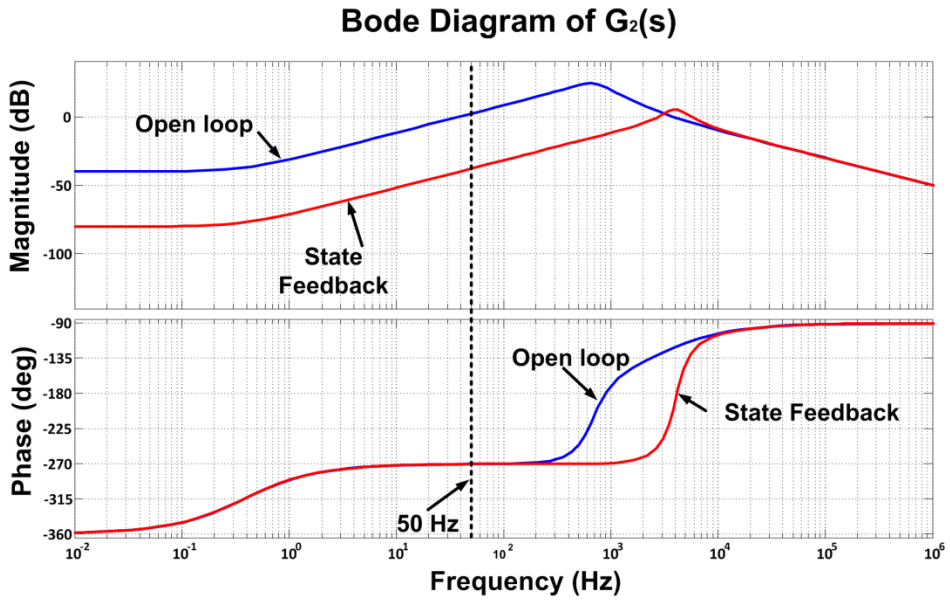

Fig. 2. (a) Open loop and closed loop Bode diagram of $G_1(s)$,

(b) Open loop and closed loop Bode diagram of $G_2(s)$.

(a)

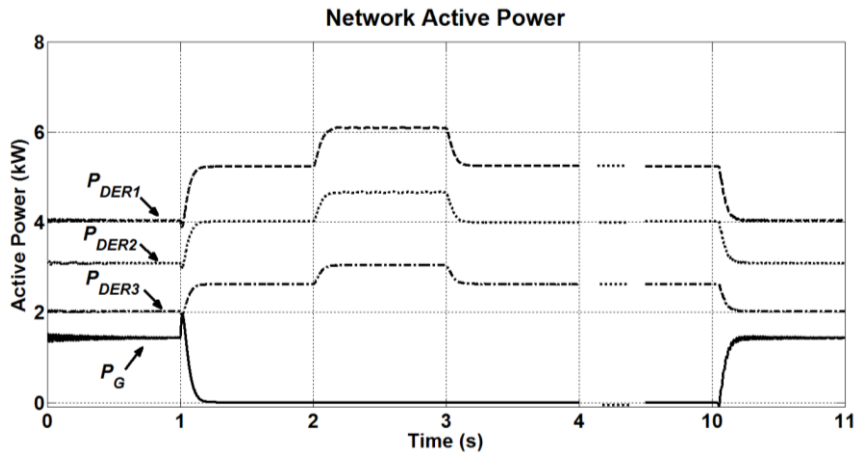

(b)

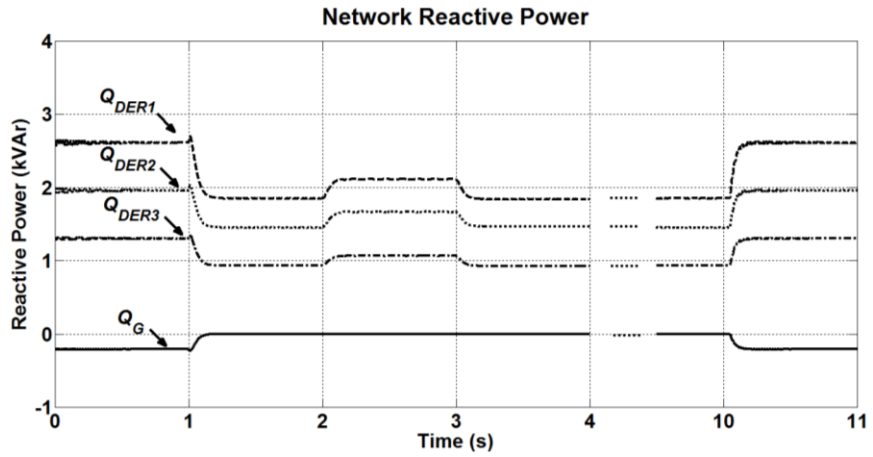

(c)

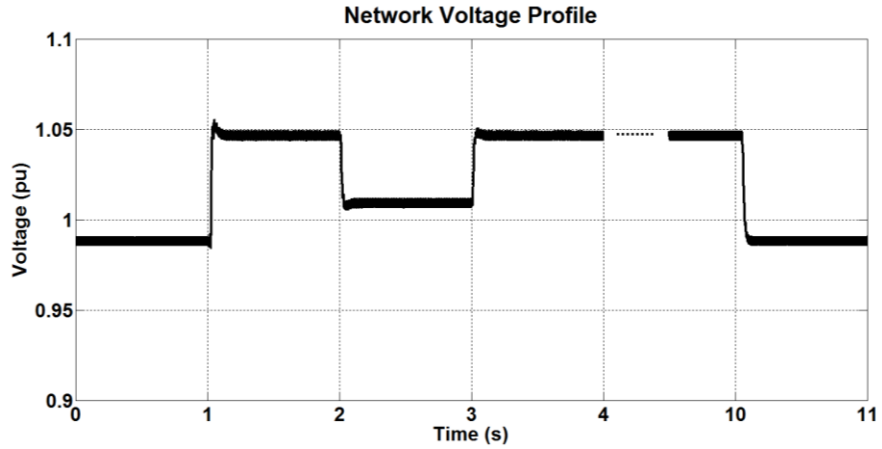

Fig. 3. Simulation results for MG–1 in case 1 before DSTATCOM connection:

(a) Active power dispatch of grid and DERs,

(b) Reactive power dispatch of grid and DERs,

(c) Network voltage profile monitored in the secondary side of distribution transformer.

(a)

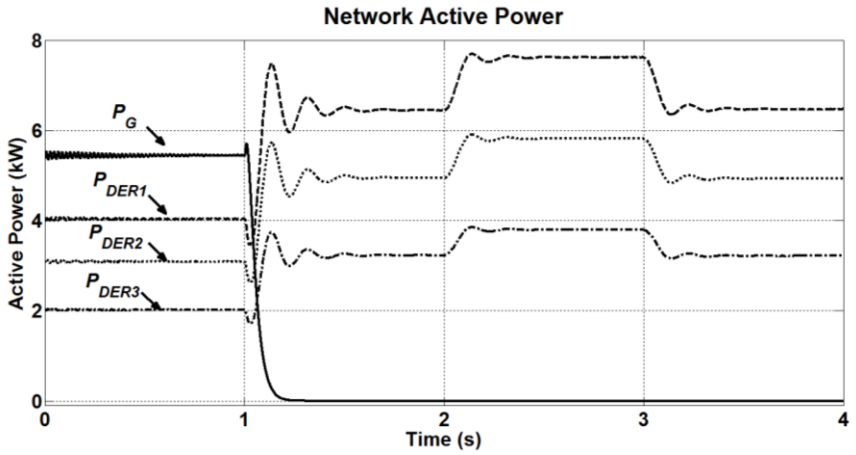
Network Active Power
Active Power (kW)
Time (s)
P_G
P_{DER1}
P_{DER2}
P_{DER3}

(b)

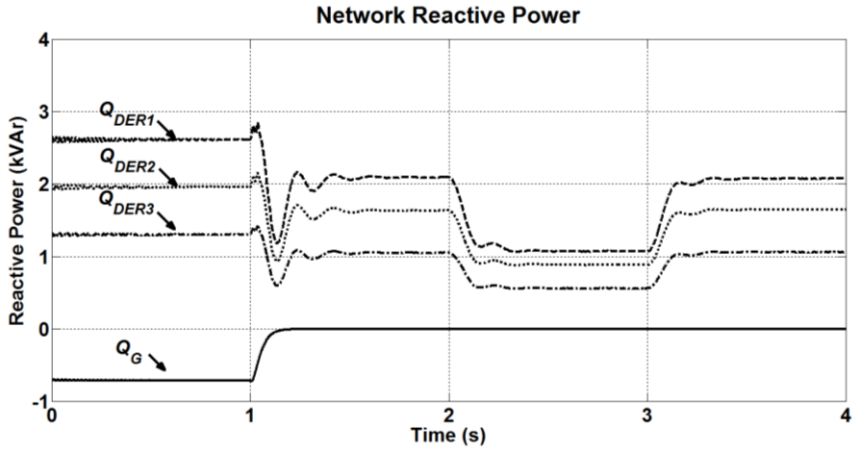
Network Reactive Power
Reactive Power (kVAr)
Time (s)
Q_{DER1}
Q_{DER2}
Q_{DER3}
Q_G

(c)

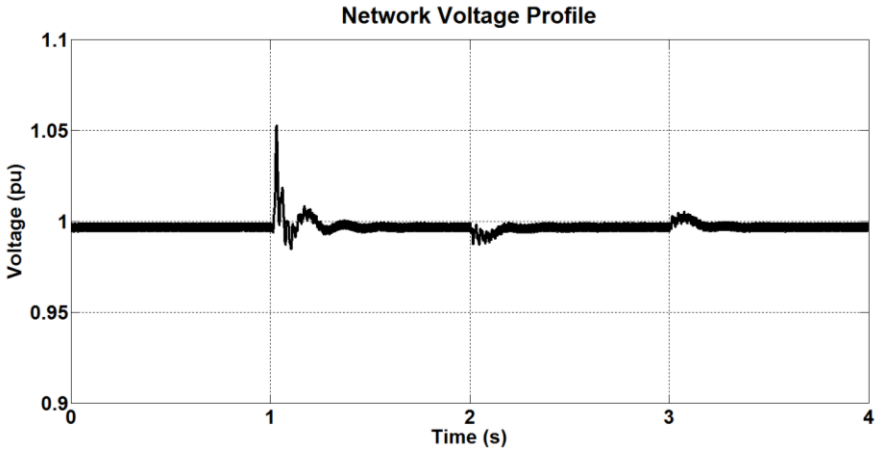
Network Voltage Profile
Voltage (pu)
Time (s)

(d)

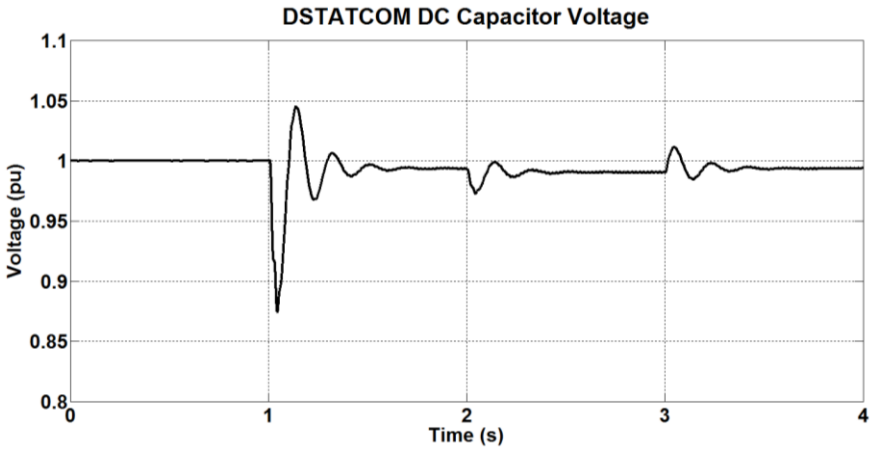

(e)

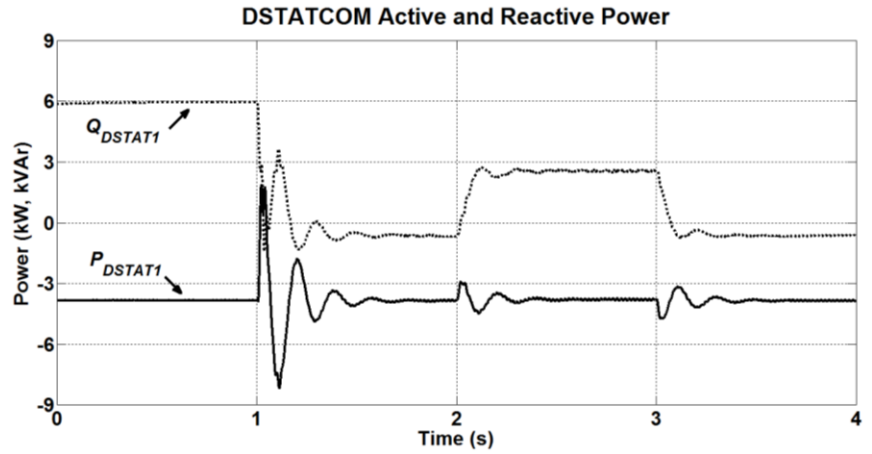

Fig. 4. Simulation results of MG–1 in case 1 after DSTATCOM connection:

(a) Active power dispatch of grid and DERs,

(b) Reactive power dispatch of grid and DERs,

(c) Network voltage profile monitored in the secondary side of distribution transformer,

(d) DSTATCOM output active and reactive power injection,

(e) Voltage profile of DSTATCOM DC capacitor.

(a)

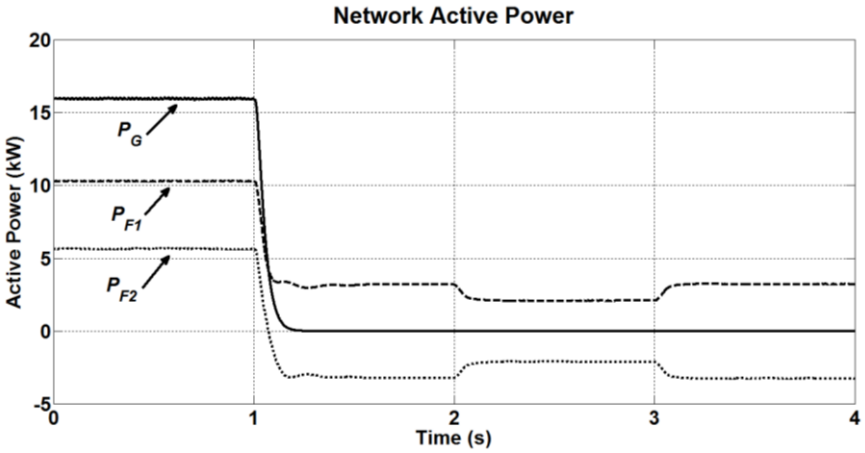
Network Active Power
Active Power (kW)
Time (s)
P_G
P_{F1}
P_{F2}

(b)

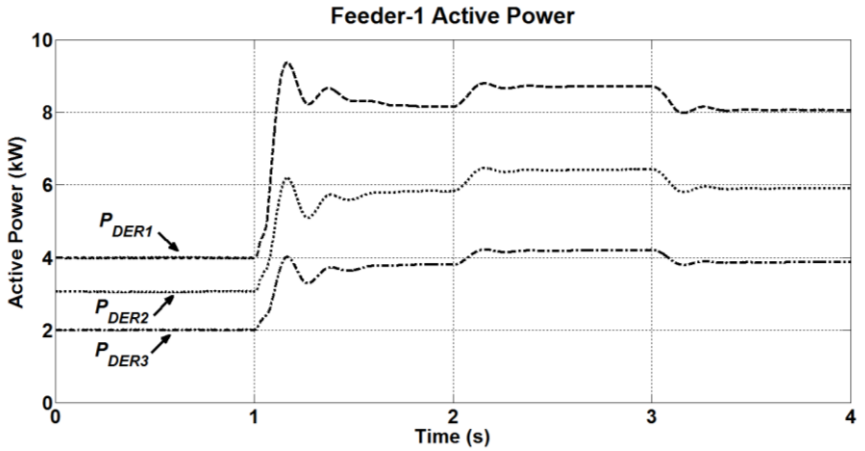
Feeder-1 Active Power
Active Power (kW)
Time (s)
P_{DER1}
P_{DER2}
P_{DER3}

(c)

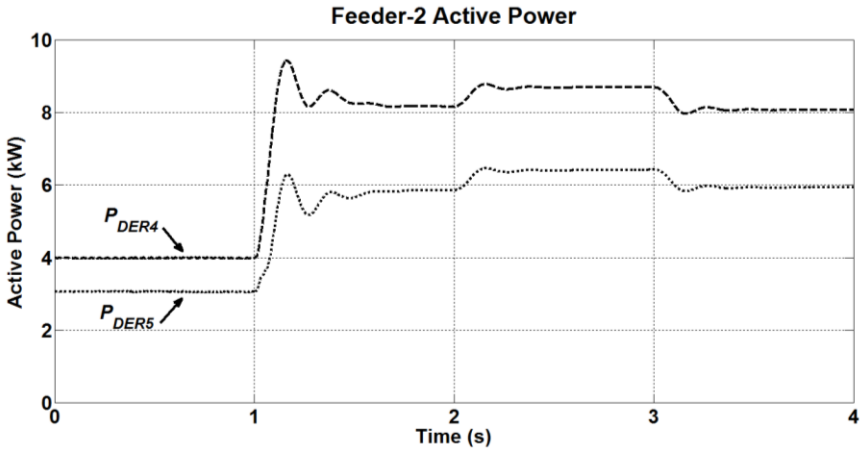
Feeder-2 Active Power
Active Power (kW)
Time (s)
P_{DER4}
P_{DER5}

(d)

(e)

(f)

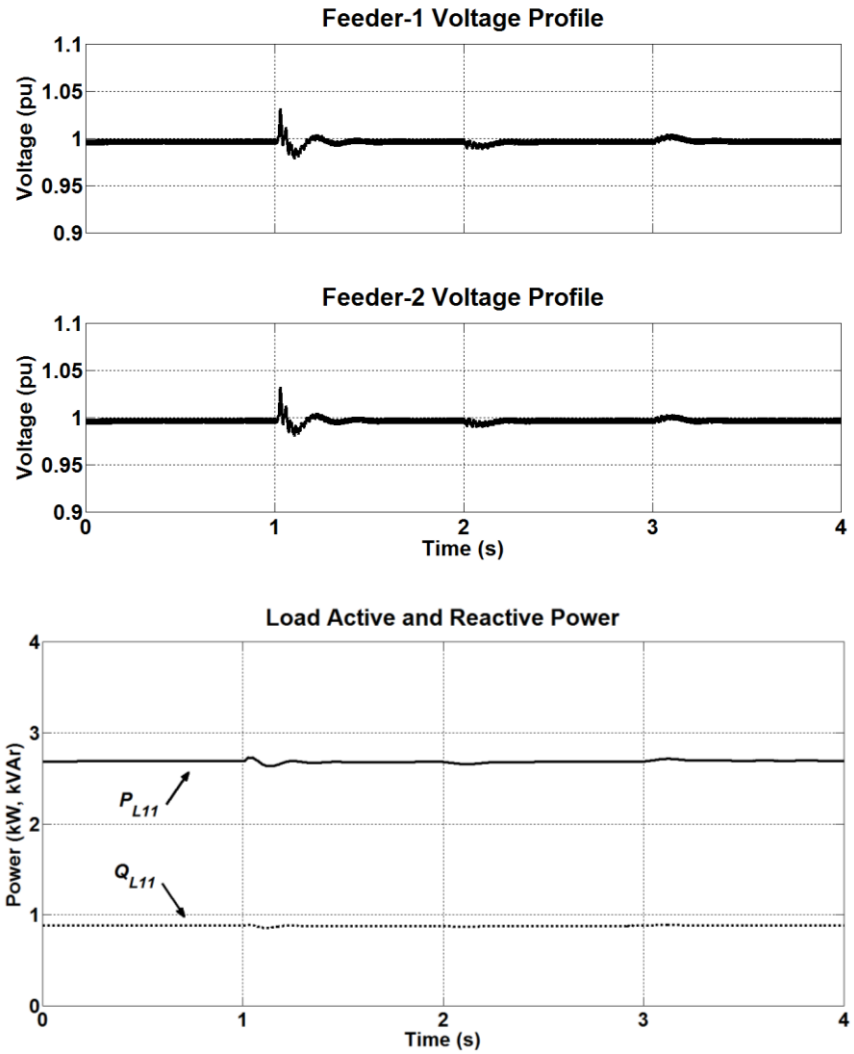

Fig. 5. Simulation results for system of interconnected MG–1 and MG–2 in case 2:

(a) Active power supply from grid and active power flow into each microgrid feeder,

(b) Active power output of each DER in MG–1,

(c) Active power output of each DER in MG–2,

(d) MG–1 voltage profile monitored in the secondary side of distribution transformer,

(e) MG–2 voltage profile monitored in the secondary side of distribution transformer,

(f) Active and reactive power demand of a sample load.

(a)

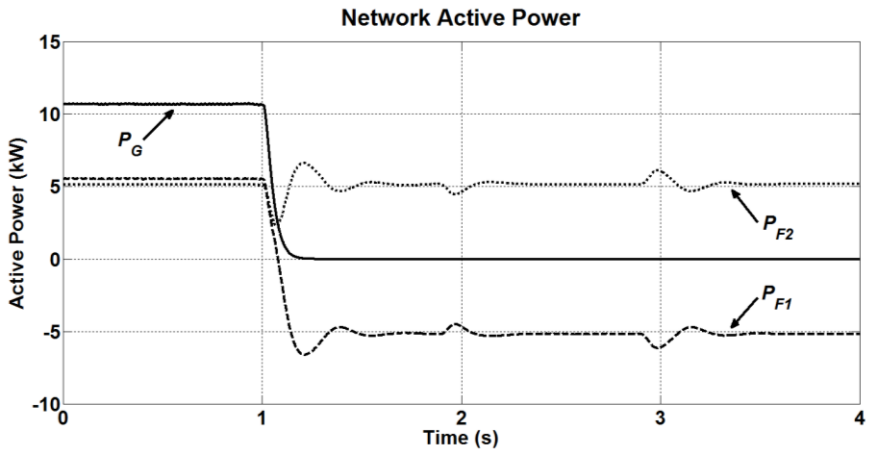

(b)

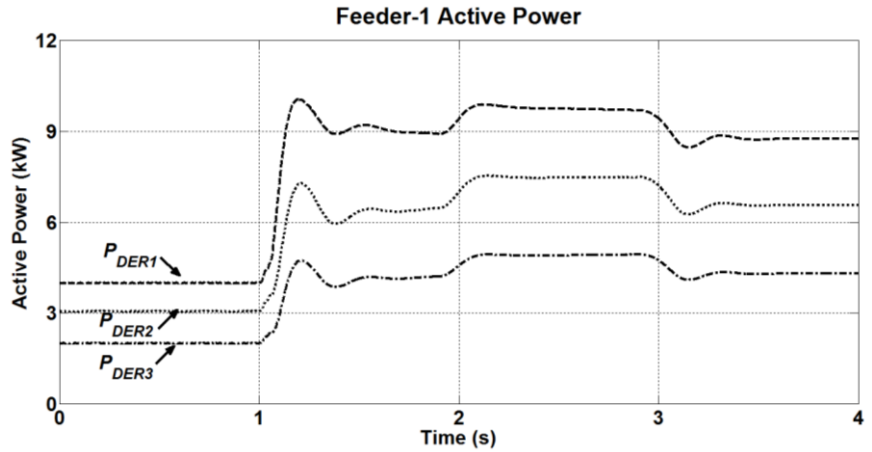

(c)

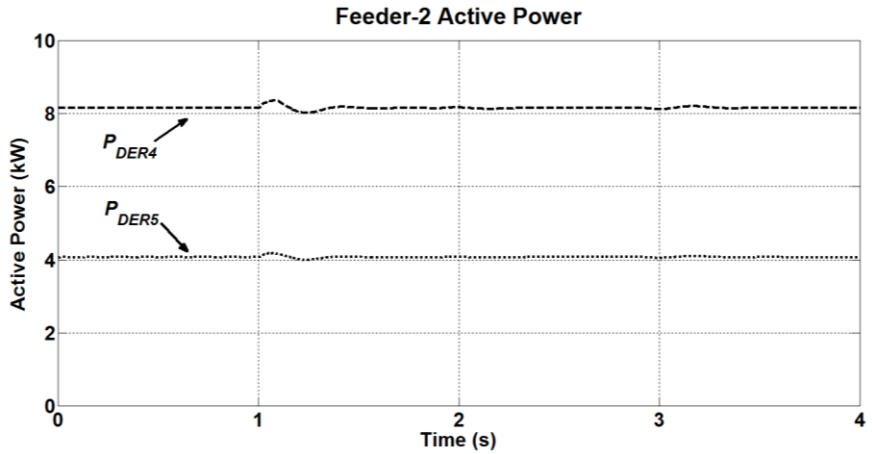

Fig. 6. Simulation results for the system of interconnected MG–1 & MG–2 in case 2 when MG–2 DERs operate in their maximum capacity:

(a) Active power supply from grid and active power flow into each microgrid feeder,

(b) Active power output of each DER in MG–1,

(c) Active power output of each DER in MG–2.

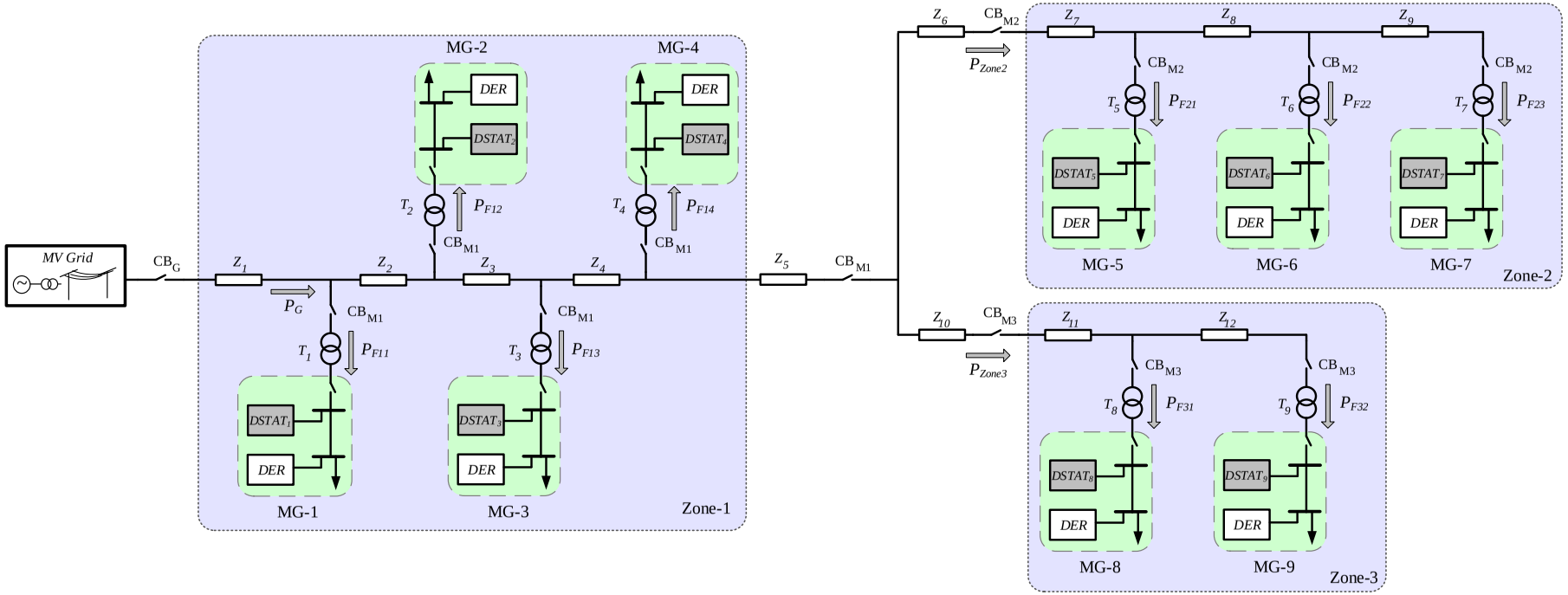

Fig. 7. Schematic diagram of the large MV feeder with self–healing capability containing several interconnected microgrids.

(a)

(b)

(c)

(d)

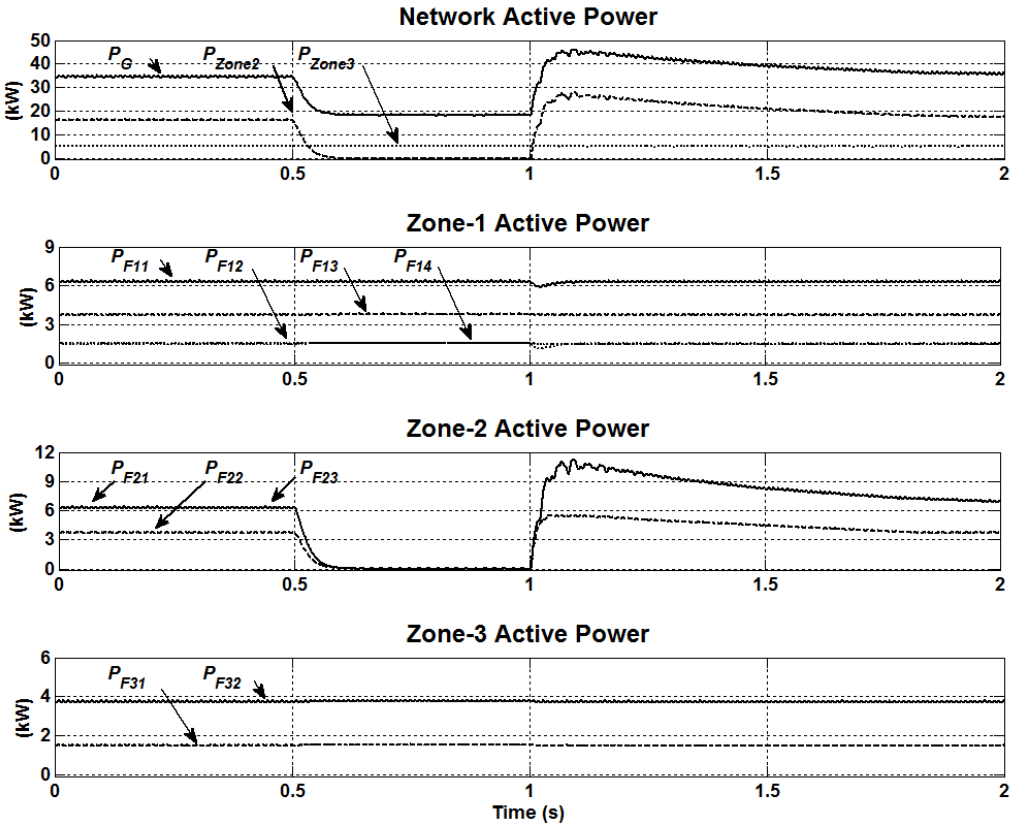

Fig. 8. Simulation results for the network in case 3.1:

(a) Active power supply from grid and active power flow into Zone–2 and Zone–3,

(b) Active power flow into each microgrid within Zone–1,

(c) Active power flow into each microgrid within Zone–2,

(d) Active power flow into each microgrid within Zone–3.

(a)

(b)

(c)

(d)

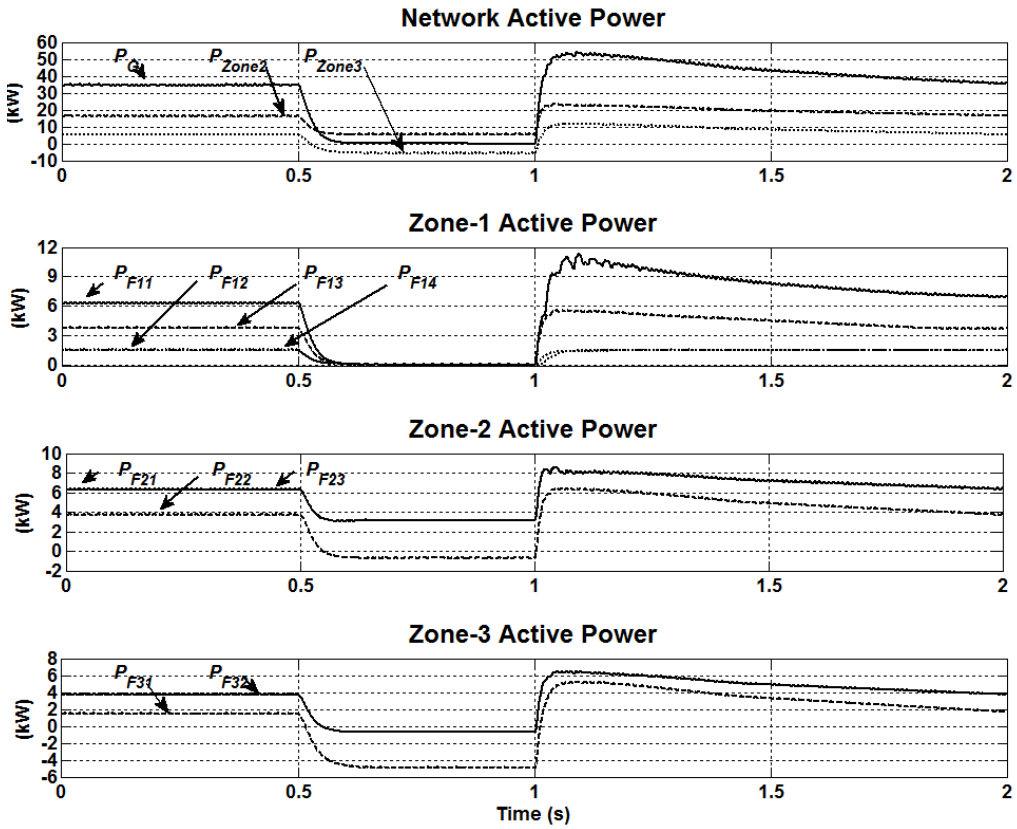

Fig. 9. Simulation results for the network in case 3.2:

(a) Active power supply from grid and active power flow into Zone–2 and Zone–3,

(b) Active power flow into each microgrid within Zone–1,

(c) Active power flow into each microgrid within Zone–2,

(d) Active power flow into each microgrid within Zone–3.

(a)

(b)

(c)

(d)

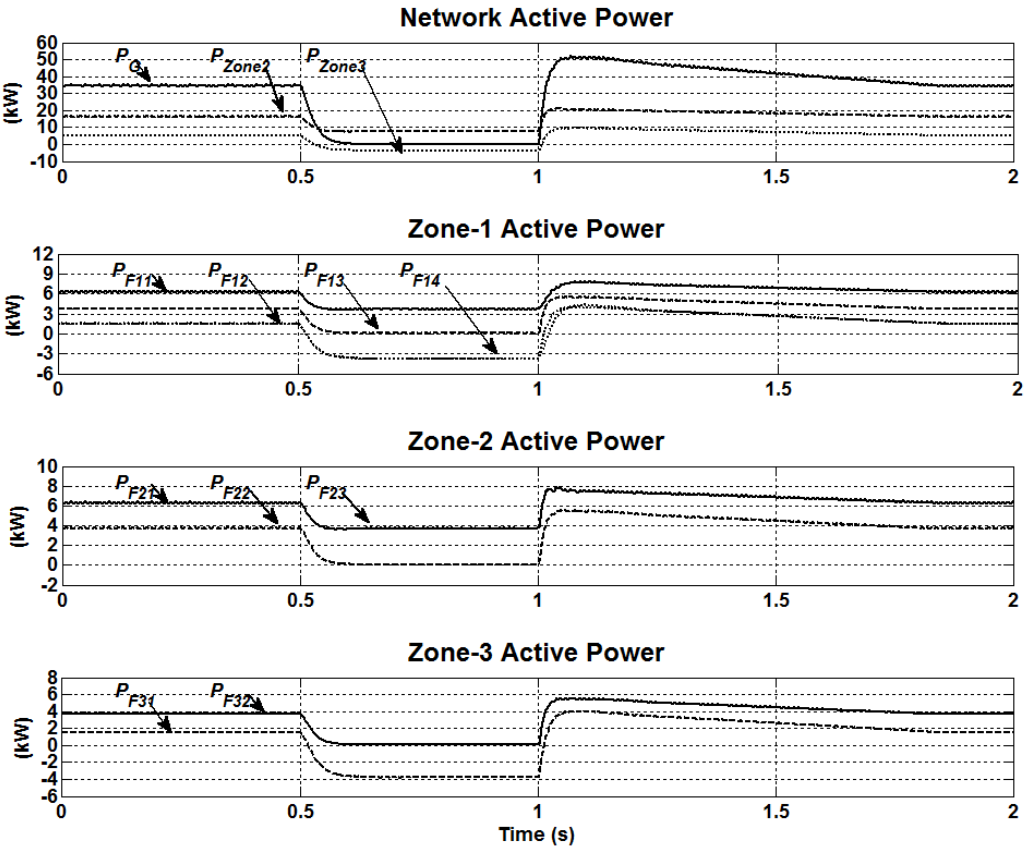

Fig. 10. Simulation results for the network in case 3.3:

(a) Active power supply from grid and active power flow into Zone–2 and Zone–3,

(b) Active power flow into each microgrid within Zone–1,

(c) Active power flow into each microgrid within Zone–2,

(d) Active power flow into each microgrid within Zone–3.